Micromachining Technologies

for MEMS fabrication

Carmen Moldovan

SILICON MICROMACHINING

- INTRODUCTION
- BULK MICROMACHINING
- SURFACE MICROMACHINING

POLYMER MICROMACHINING

GLASS MICROMACHINING

CERAMICS MICROMACHINING

INTRODUCTION

SILICON as a material for MST/MEMS

Positive:

- **Good electrical and mechanical properties e.g. elasticity, piezoresistivity**
- **Well understood characteristics**
- **Well established processing methods**
- **Integration of mechanical/electronic/optical functions**

Limitations:

- **Limited materials flexibility e.g no magnetic material, no piezoelectric**
- **Difficult interfacing - interconnections/ packaging problems still under development**
- **Limited functionality at high temperature**

MICROMACHINING TECHNOLOGY

- **Micromachining technology allows the fabrication of electro- mechanical optical structures with very small dimensions (in the micrometer range), 3D, using special processes, different of conventional IC technologies.**

- **Generally the micromachining technology can be classified in : bulk micromachining and surface micromachining**
  - ***Bulk micromachining is based on single crystal silicon etching, and the micromechanical structures developed with this technology are made of either silicon crystal or deposited or grown layers on silicon.***

- **Micromechanical structures produced by micromachining technology can be divided into three groups: static, dynamic, and kinematic.**

- **Static micromechanical structures includes free three dimensional structures such as nozzles, cavities, capillary column, circular orifices, miniature electrical connectors.**

- **Dinamic micromechanical structures: diaphragmes, membranes, microbridges, cantilever beams, resonators. They require control displacement to accomplish the desired function.**

- **The kinematic group includes micromotors, microgears, pin joints, springs, cranks, sliders. The kinematic devices ar considered to be essential in the future for microrobotics and microsurgery.**

DIMENSIONS

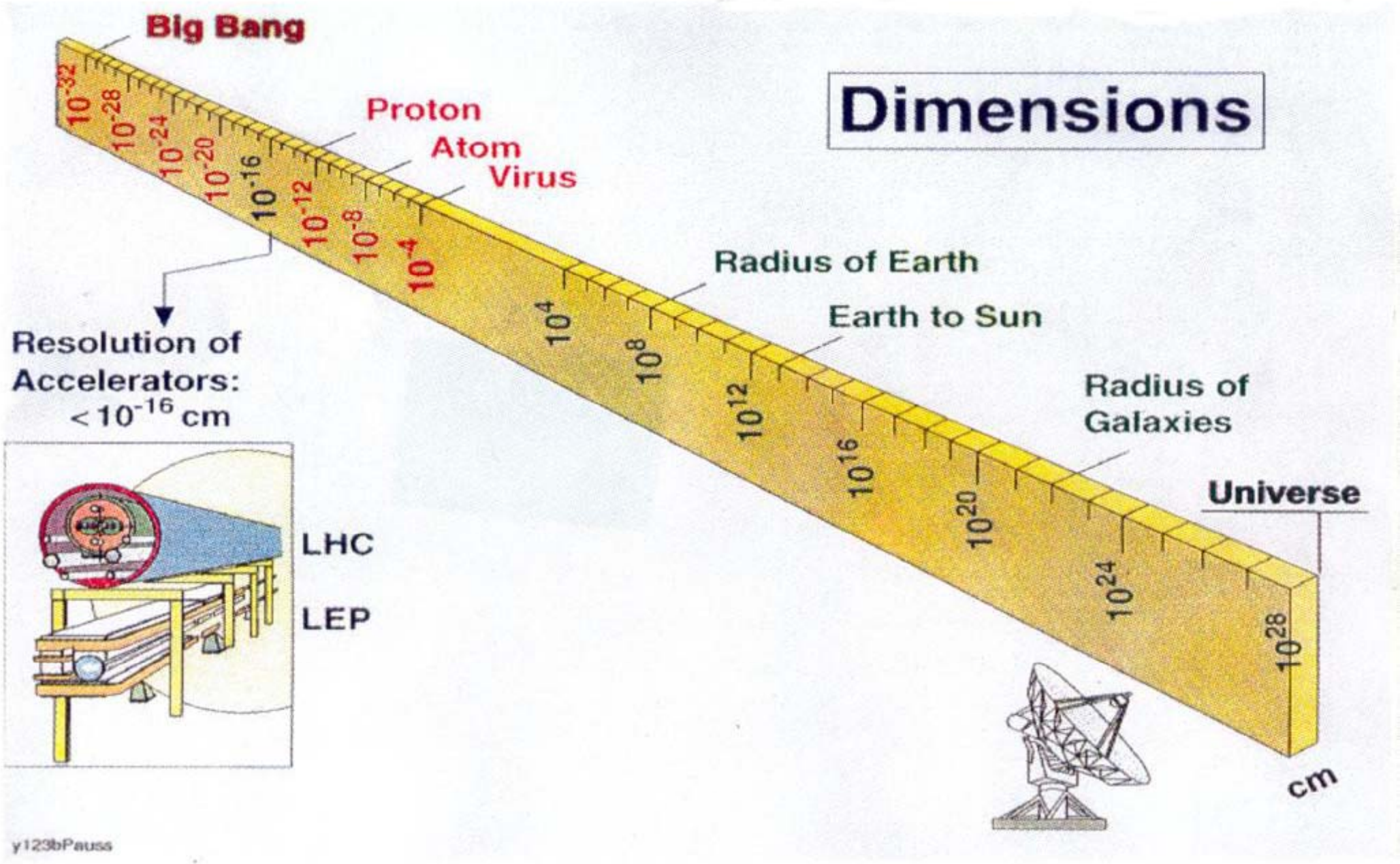
Dimensions
Big Bang
Proton
Atom
Virus
Radius of Earth
Earth to Sun
Radius of Galaxies
Universe
cm
Resolution of Accelerators: $< 10^{-16}$ cm
LHC
LEP
10^{-32}
10^{-28}
10^{-24}
10^{-20}
10^{-16}
10^{-12}
10^{-8}
10^{-4}
10^{4}
10^{8}
10^{12}
10^{16}
10^{20}
10^{24}
10^{28}
y123bPauss

MATERIALS		STRUCTURES		INFRASTRUCTURE
nano-level (10^{-9})	micro-level (10^{-6})	meso-level (10^{-3})	macro-level (10^{+0})	systems-level (10^{+3}) m
Molecular Scale	*Microns*	*Meters*		*Up to Km Scale*
*nano-mechanics	*micro-mechanics	*meso-mechanics	*beams	* bridge systems
*self-assembly	*micro-structures	*interfacial-structures	*columns	* lifelines
*nanofabrication	* smart materials	*composites	*plates	*airplanes

Fig. 1. Physical scales in materials and structural systems

BORESI AND CHONG, *ELASTICITY IN ENGINEERING MECHANICS*, WILEY, 2000.

Bulk micromachining = 3D configuration technique of silicon and thin films by using specific processes: chemical and electrochemical anisotropic etching, stop etch technique, assisted laser technique, anodic bonding, double side alignment, LIGA technique.

Bulk micromachining of silicon is based mainly on anisotropic etching. This relies on the fact that certain aqueous alkaline solutions attack silicon at widely differing speeds in the various crystallographic directions

Silicon crystallographic directions

Crystallographic Structure
is a diamond type cristal with centrated faces, and a constant lattice of 5,43 A

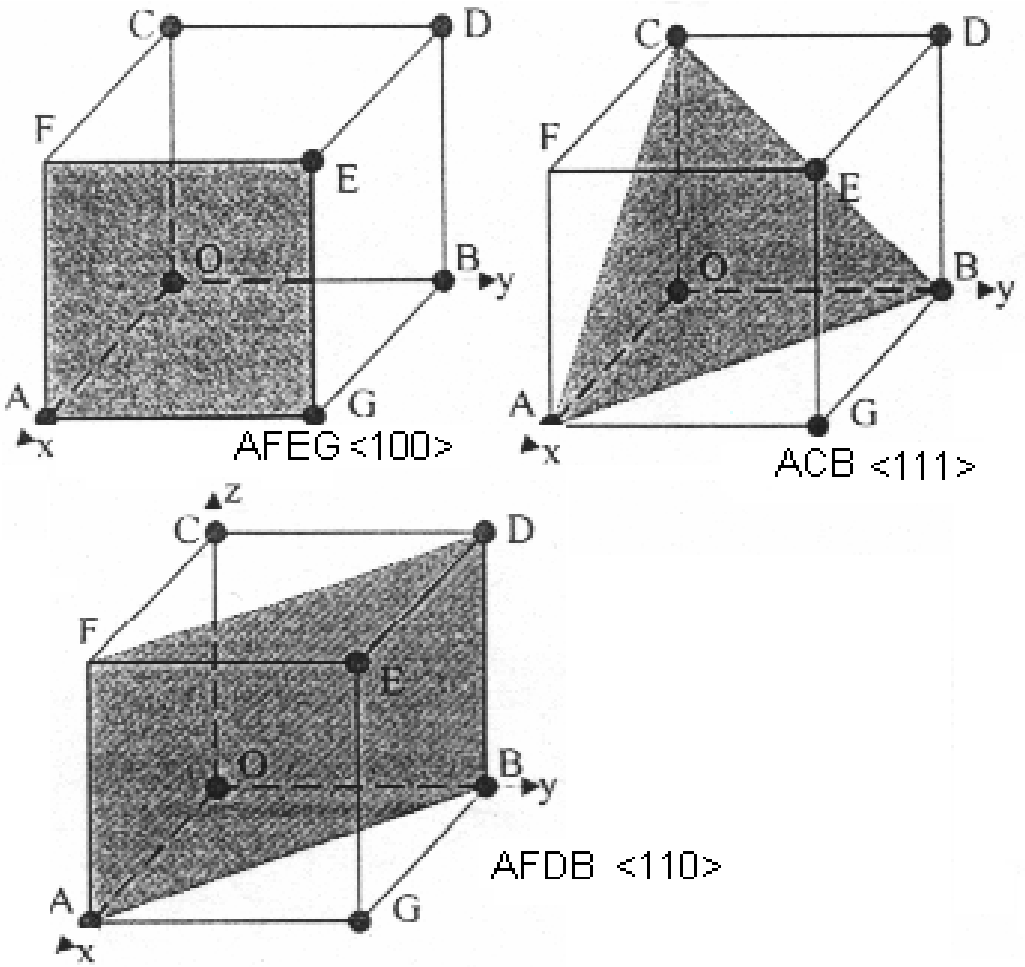

Crystallographic orientation – Dependent Etch rate

A basic feature of anisotropic etchants is that their etch rates are dependent of the crystallographic planes. <111> surfaces etch at a slower rate than all other crystallographic planes. This indicates that the dissolution rate will be a function of the crystal orientation of the silicon rate. Anisotropic etching is a function of the density of atoms (number of atoms per square centimetre), the energy needed to remove an atom from the surface, and geometric screening effects (three-dimensional distribution of atoms in the lattice). As a consequences of anisotropy it is possible to develop unique structures not otherwise feasible.

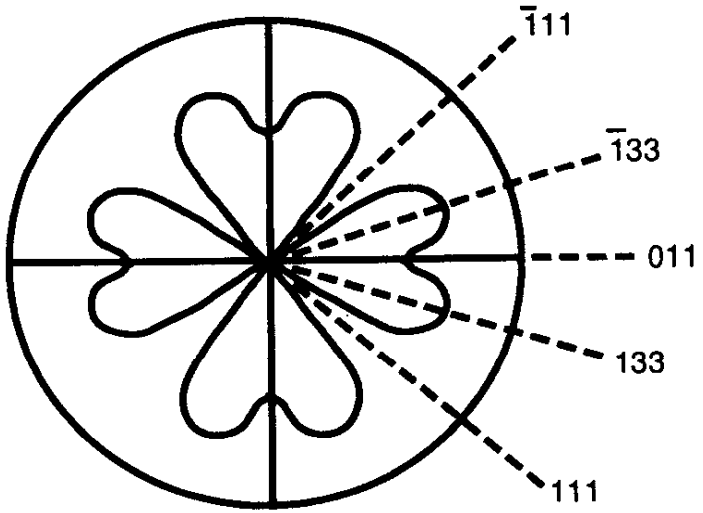

EDP etch rate dependence on crystallographic orientation in <100> silicon.

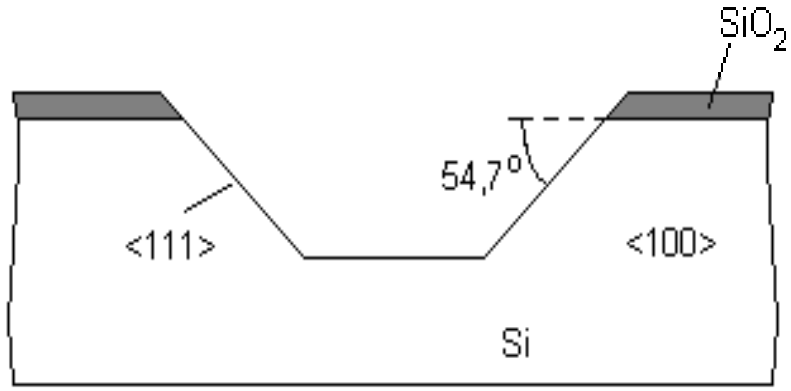

Truncated pyramidal pit bounded by silicon <111>planes

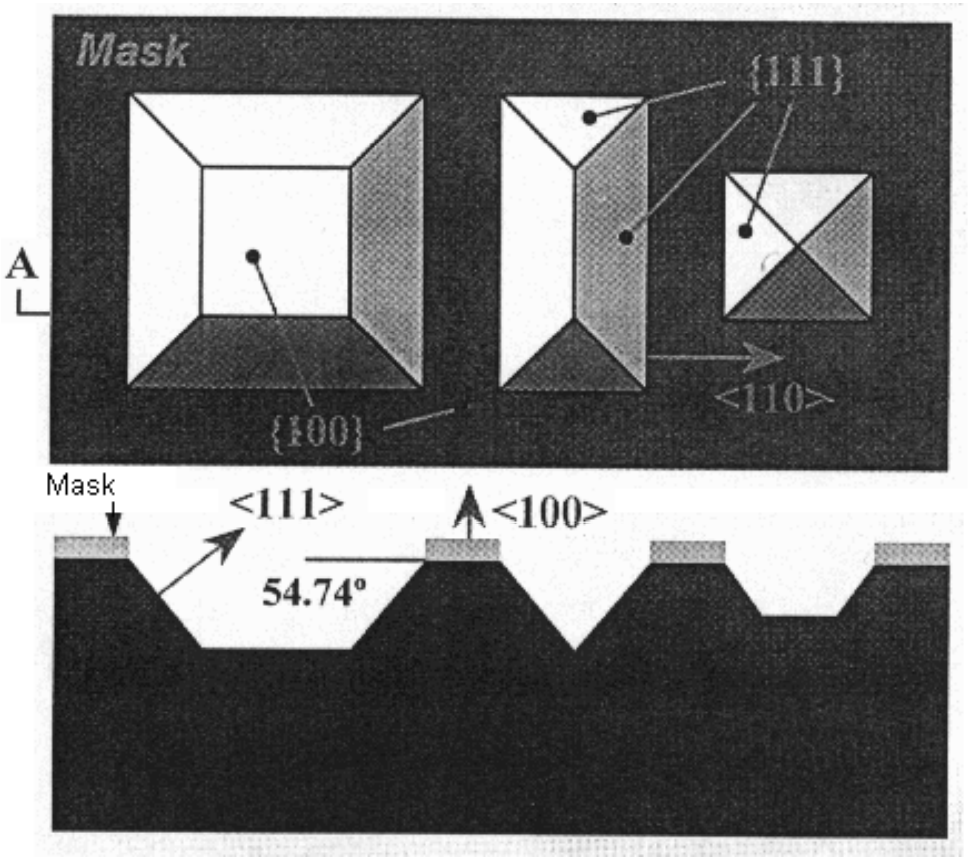

Etching profile for Silicon <100> anisotropically etched

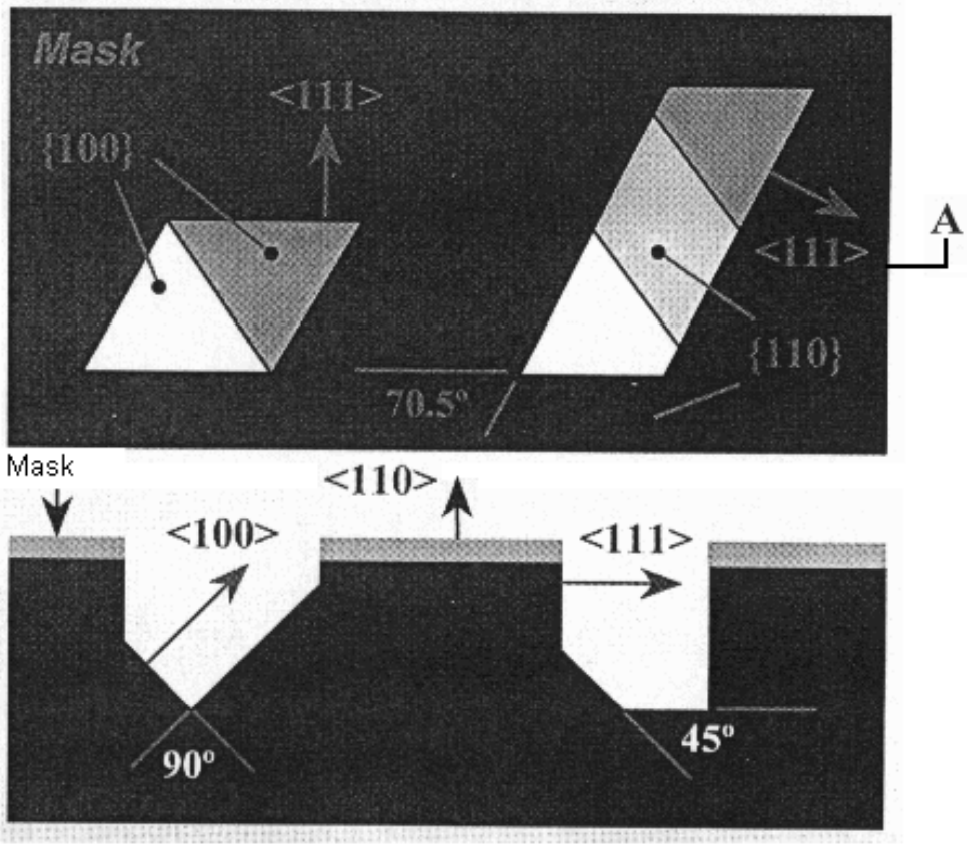

Etching profile for Silicon <110> anisotropically etched

Lithographic Process

Bulk micromachining technique

A. Oxidation

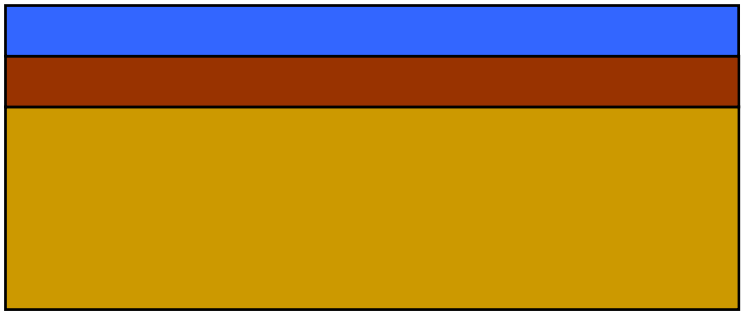

B. Litography preparation

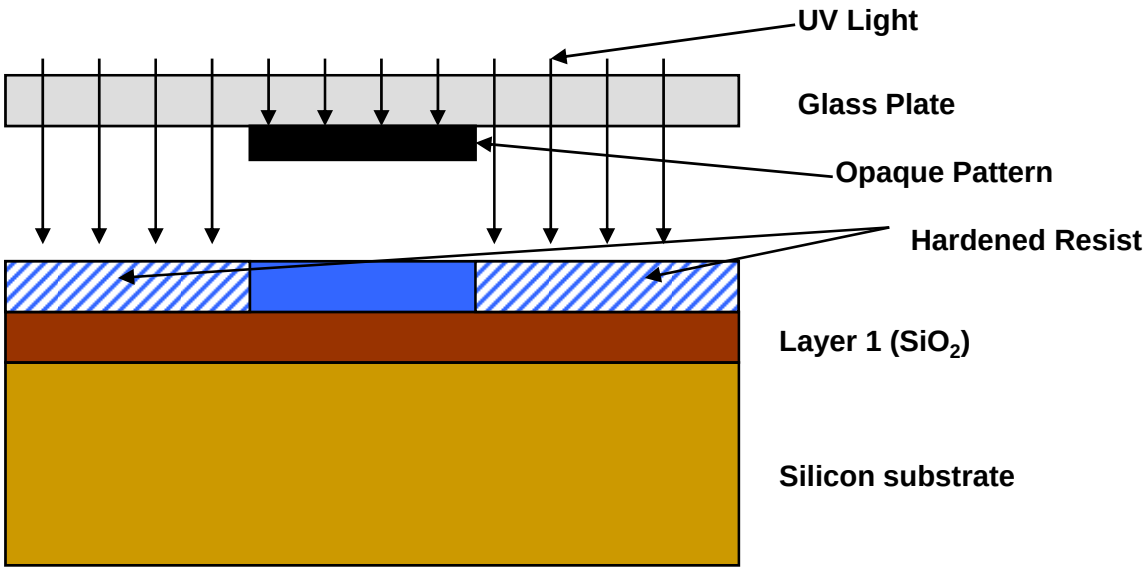

C. Exposure

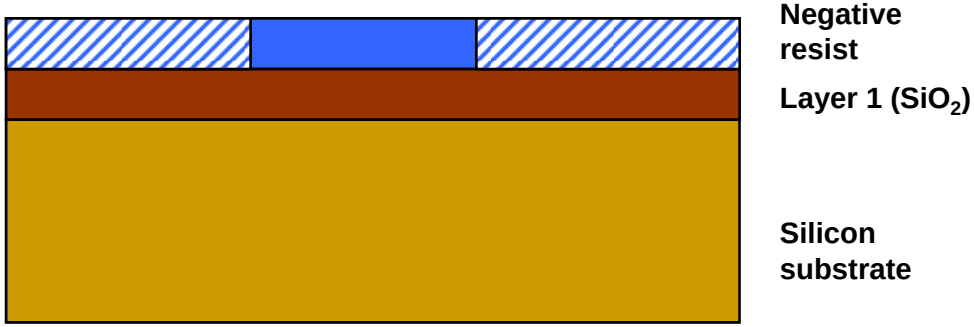

D. Unexposed Photoresist Removed by Developer

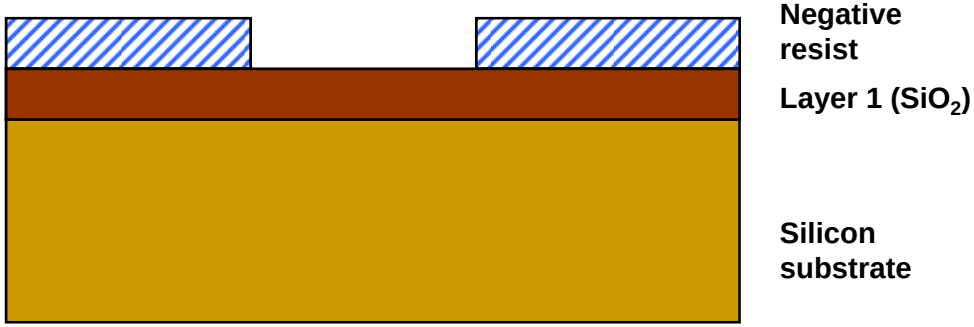

E. SiO_2 etched with NH_4F + HF

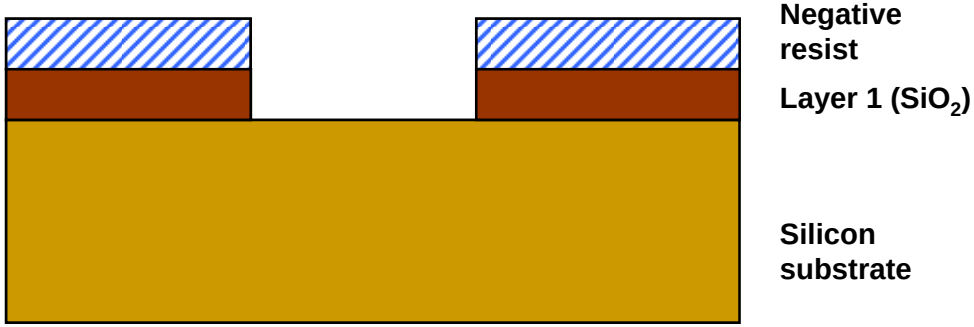

F. Exposed Photoresist Removed with H_2SO_4

SILICON BULK MICROMACHINING

- Anisotropic etching
- Double side alignment
- Laser machining
- Anodic Bonding

SILICON ANISOTROPIC ETCHING

Anisotropic etching of silicon was studied as a function of:

- *Orientation of monocrystaline silicon*
- High dose boron concentration
- Etchant temperature
- *Composition and concentration of the etchant*

The most important anisotropic etchants of silicon

- *Hydroxides of alkaline metals: KOH, NaOH, LiOH, CsOH*
- *Diamines:EDP(Ethylenediamine-pyrocatechol-Water)*
- *Tetramethylammonium Hydroxide (TMAH)*

ANISOTROPIC ETCHING OF SILICON

KOH (potassium hydroxide) – high etch rate, strong alkaline character, high dependence of the etching rate on the crystallographic orientation and boron concentration of the substrate

Up to now, two aspects of the silicon etching have been generally accepted /3.1/, /3.2/:

a) The general reaction:

$$Si + 2H_2O + 2HO^- \rightarrow SiO_2(OH)_2^{2-} + 2H_2$$

b) The intrinsic etching process steps:

b1. Diffusion of the reactant molecules through the boundary layer to the silicon surface;

b2. Adsorption of reactant molecules on the solid surface of silicon;

b3. Surface reaction;

b4. Reaction product desorbtion;

b5. Diffusion of by-products back across the boundary layer into the bulk of the solution

Potassium Hydroxide - KOH

1) The highest etch rate has been obtained for a concentration of 10 - 15% simple KOH and ~ 30% KOH + isopropylic alcohol. The isopropylic alcohol in KOH solution leads to the decrease of the etch rate and of the boiling temperature of the solution.

2) No effect of the etchant stirring has been found ⇒ the reaction is not limited by the diffusion

3) The ration between the etch rates of the silicon directions Si<100>/Si<111> is 35:1

Seidel

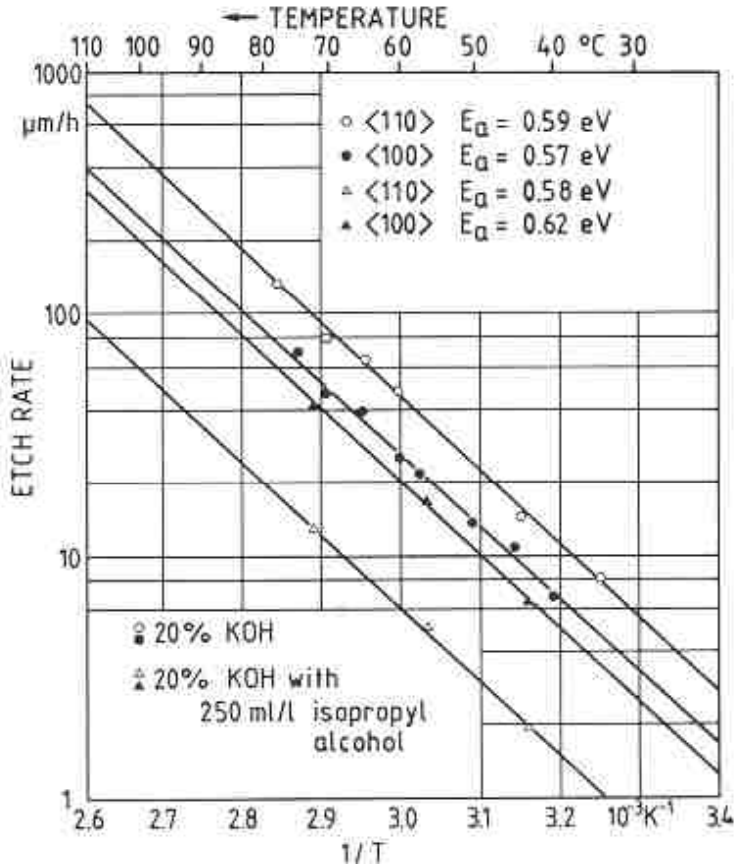

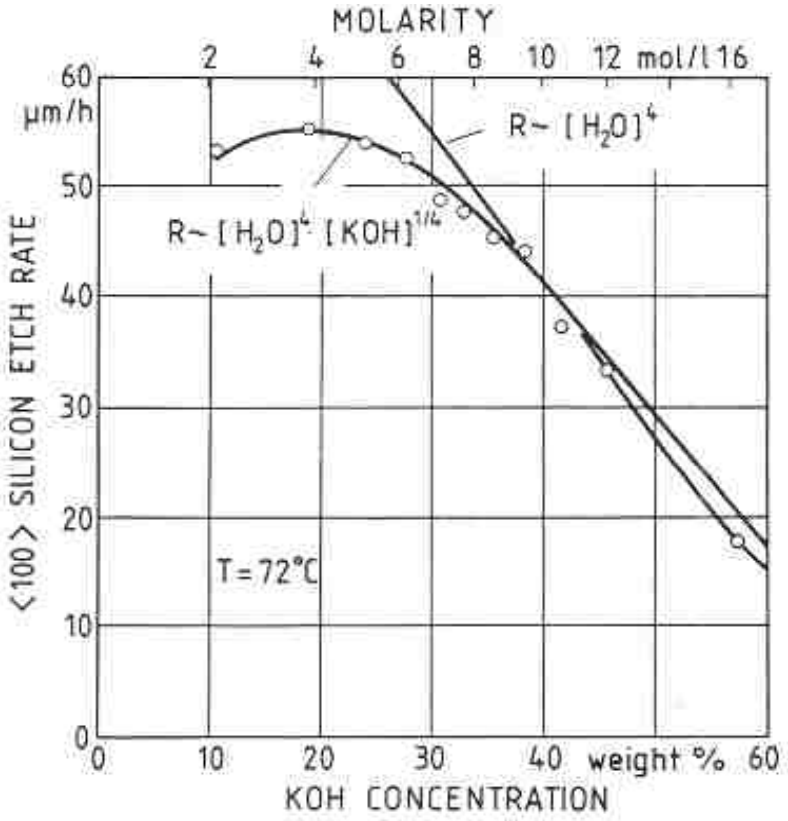

Ethylendiamine – pyrocathecol –water (EDP)

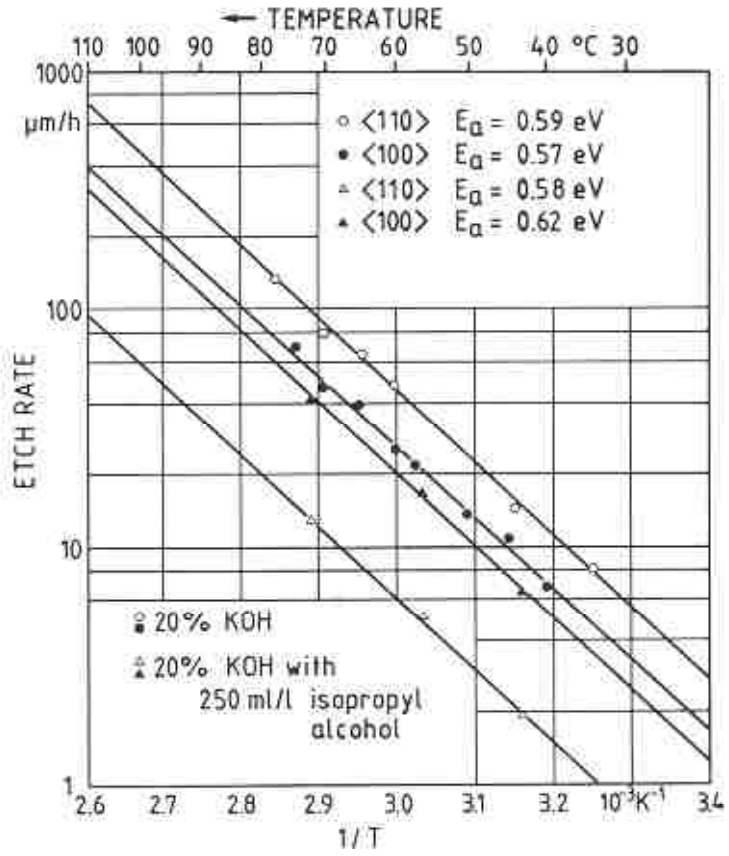

Si etch rate in EDP, after Seidel /2.2/

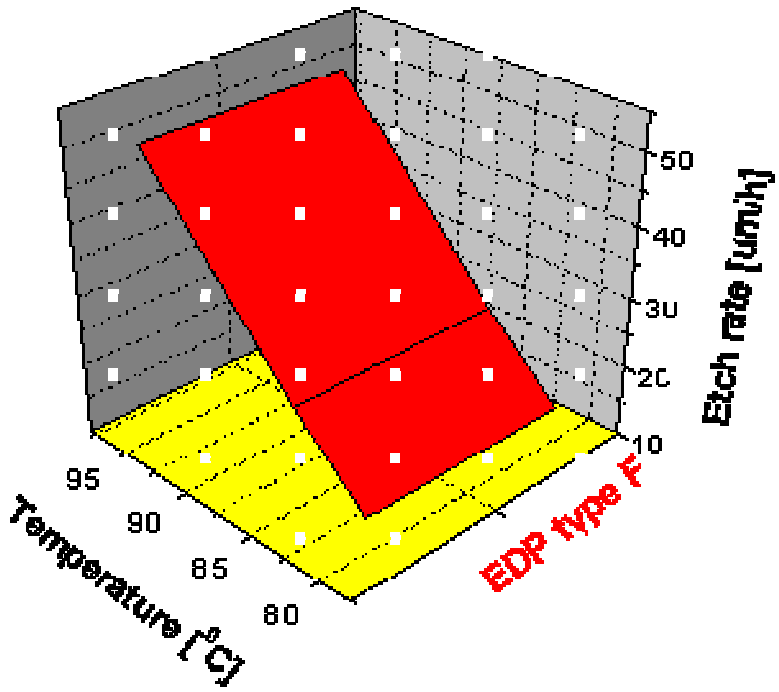

Si etch rate in EDP – experimental/2.5/

Ethylendiamine – pyrocathecol

- **The micropyramides are related to the plan <111>, one characteristic of all the anisotropic etchants used for experiment and study.**
- **Changing the composition of etchants, it is possible to modified the density and the size of micropyramides**
- **Micropyramides are the results of the anisotropy of the solution, they appear together, the smallest are situated on one of the pyramid side, and make that the edge of the pyramid base to be curved, not right.**

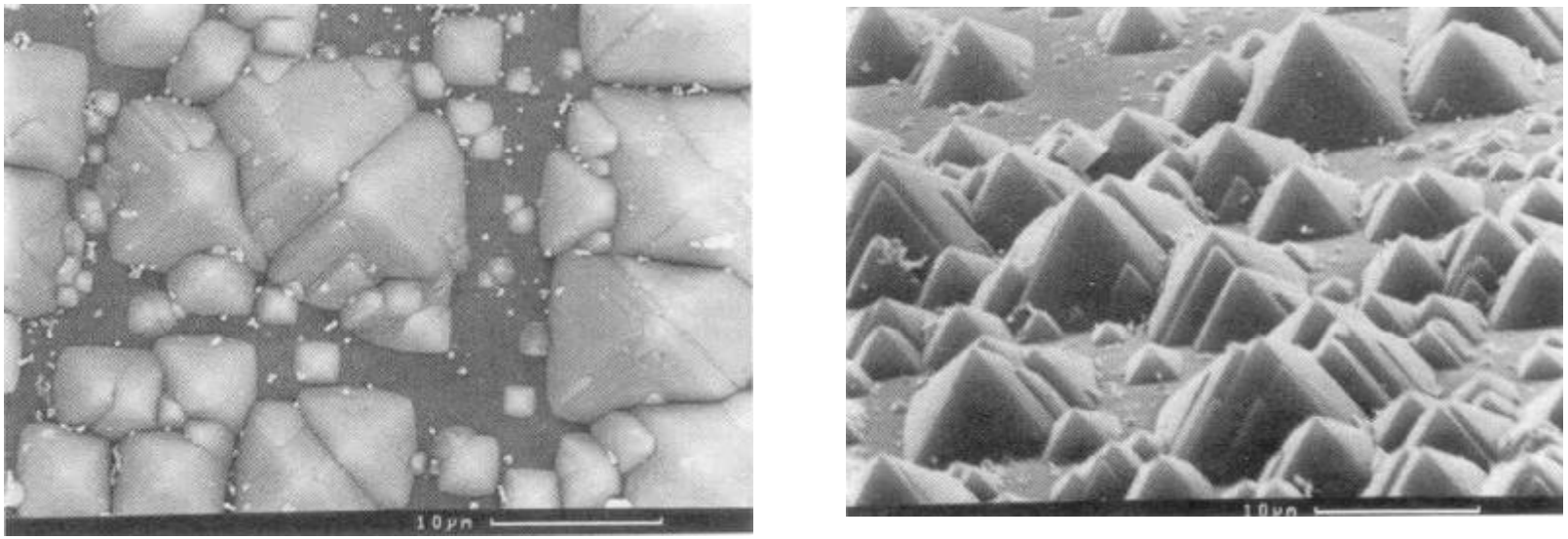

Fig.2. 5. Silicon hillocks during the anisotropic etching in EDP /Tan/.

AFM Investigation of silicon wafer roughness after the anisotropic etching process

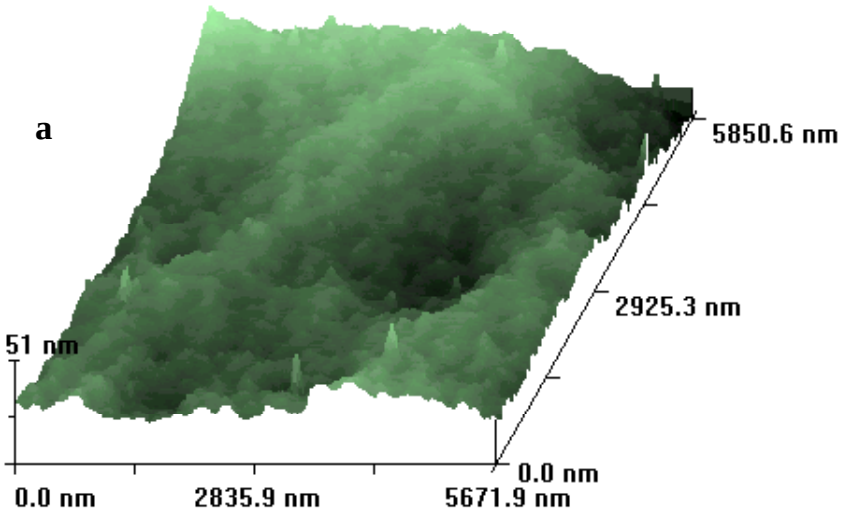

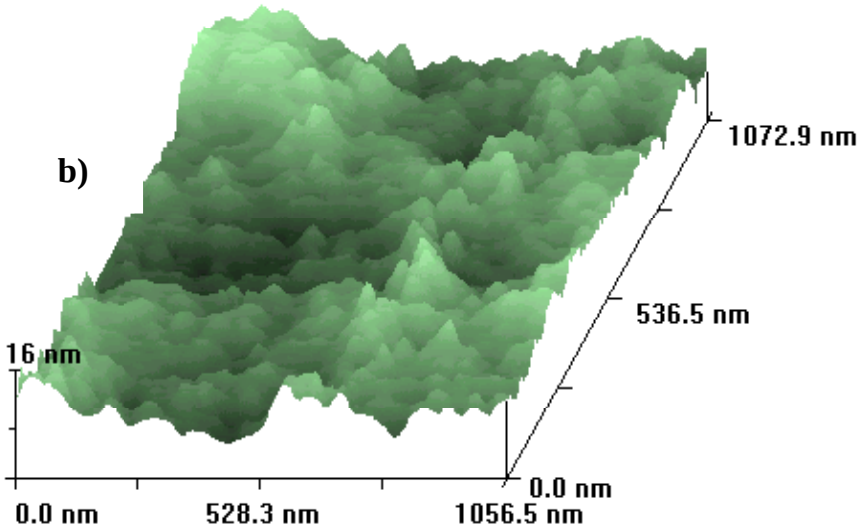

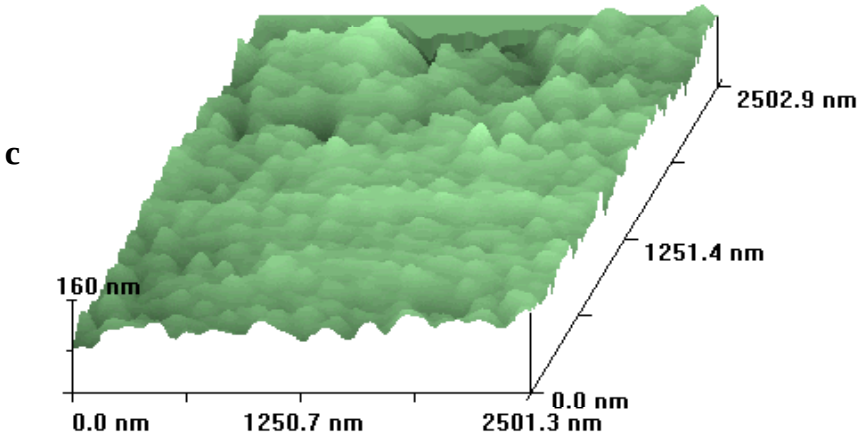

Roughness of a silicon wafer 200μm thickness, etched in 4.5M KOH+ redox system + complexant, at 80^0C (3D-AFM investigation): a) calix[4]arene complexant; b) ether crown complexant; c) simple 4.5M KOH

HILLOCKS MINIMIZATION ON THE SILICON SURFACE

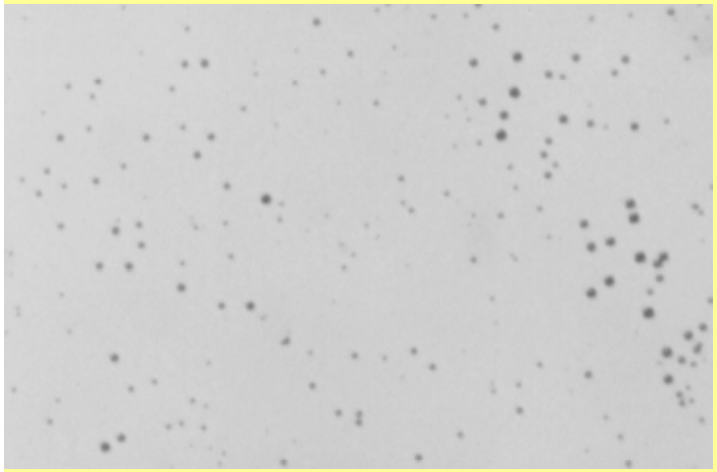

a) 10^{-2} [M/l] phenol concentration

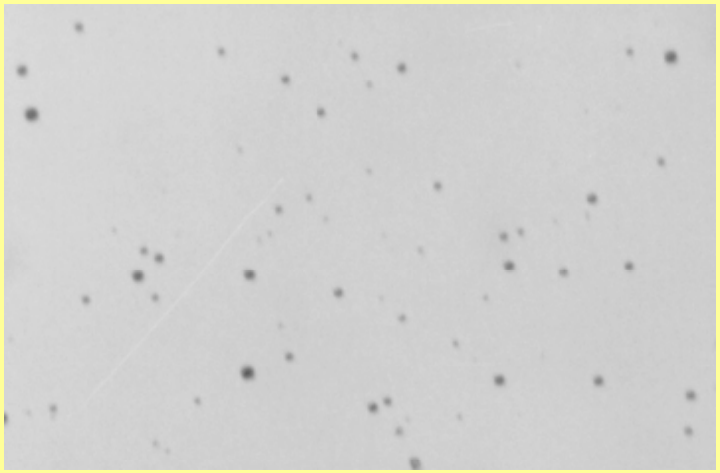

b) 10^{-3} [M/l] phenol concentration

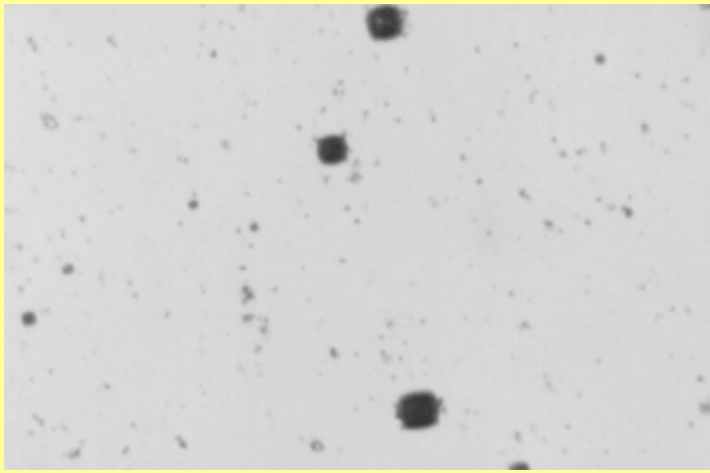

c) 10^{-4} [M/l] phenol concentration

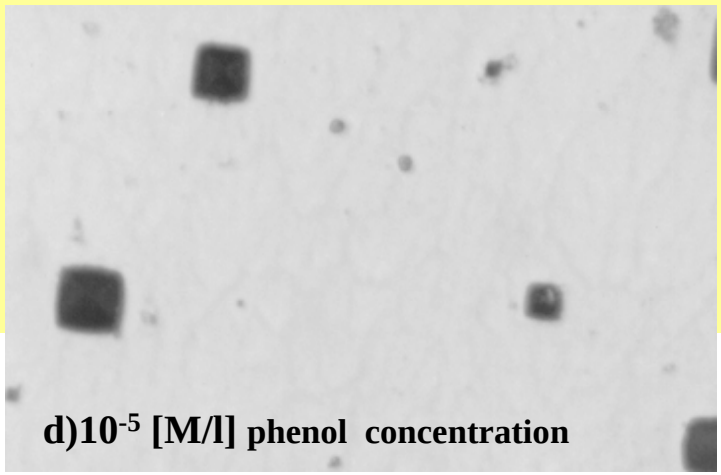

d)10^{-5} [M/l] phenol concentration

Fig. 2.11. a, b, c, d Top view microscop picture of n type <100> Si etched 1h at 85^0C in 4.5M KOH+ phenol at different concentration

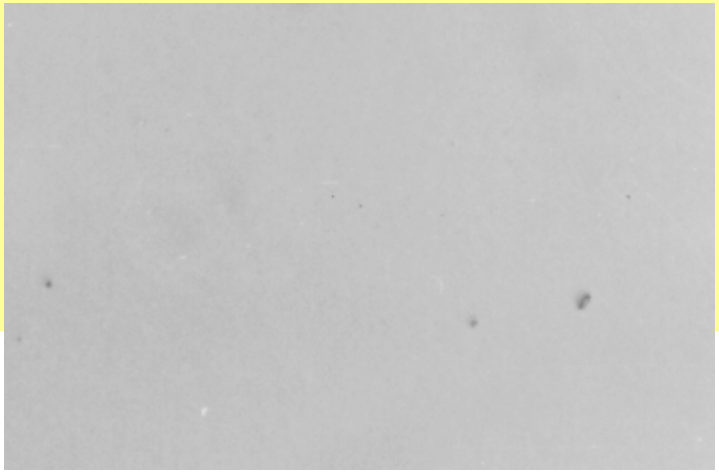

Fig.2.12. Top view microscop picture of n type<100> Si etched 1h at 85^0C in 4.5M KOH+ 10^{-4} M/l p-tert butylphenol

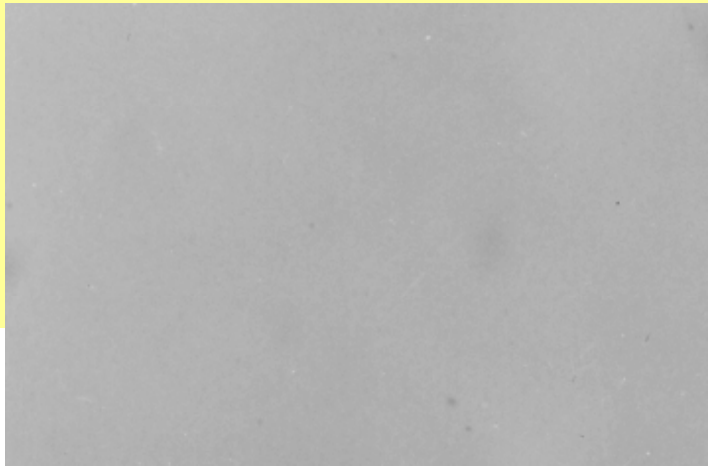

Fig.2.13.Top view microscop picture of n type<100> Si etched 1h at 85^0C in 4.5M KOH+ 10^{-5} M/l azo calix[4]arene

SILICON HILLOCKS MINIMIZATION DURING THE ANISOTROPIC ETCHING PROCESS

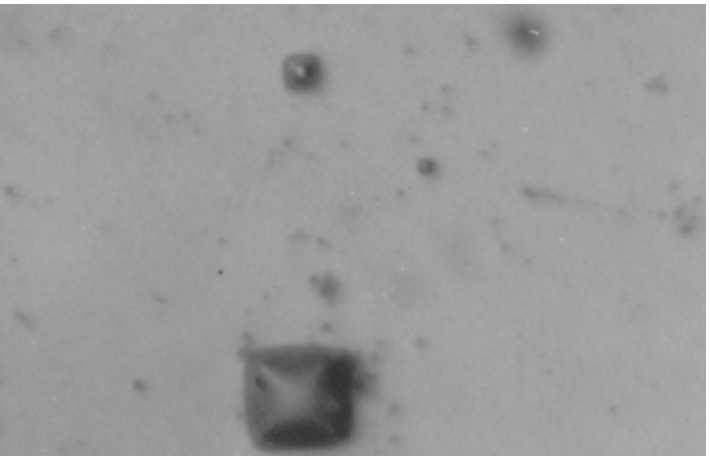

Fig.2.14. Top view microscop detail of n type<100> Si etched 1h at 85^0C in 4.5M KOH

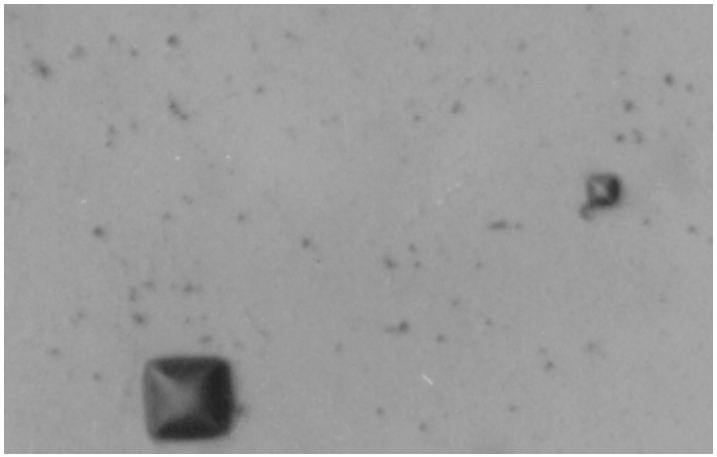

Fig.2.15. Top view microscop detail of n type<100> Si etched 1h at 85^0C in 4.5M KOH+ 10^{-4} M/l p-tert butylphenol

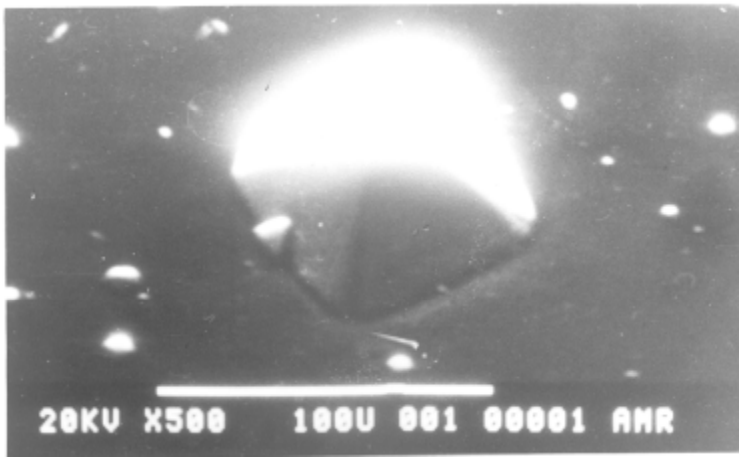

Fig.2.16. SEM picture of hillocks of silicon n<100> etched in KOH+ 10^{-4} M/l phenol

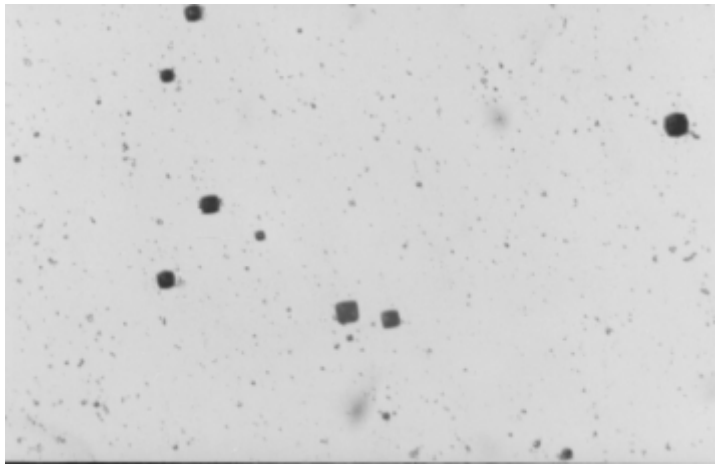

Fig.2.17. T op view microscop picture of n type<100> Si etched 1h at 85^0C in 4.5M KOH

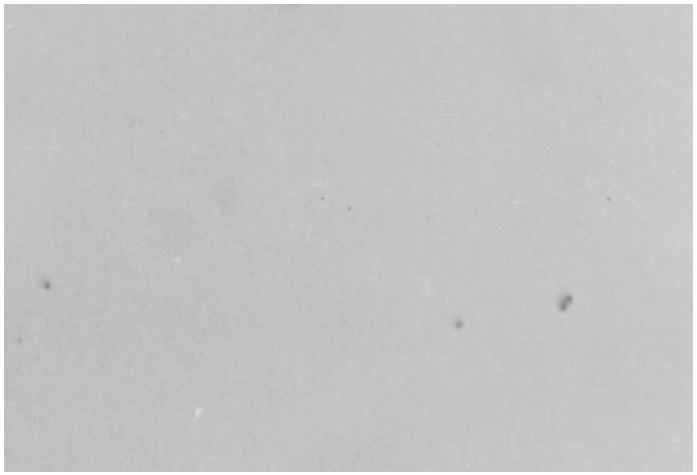

Fig.2.18. T op view microscop picture of n type<100> Si etched 1h at 85^0C in 4.5M KOH +redox system

COMPARISON STUDY OF SILICON MEMBRANE HILLOCKS FOR ANISOTROPIC ETCHING IN NaOH and $LiOH \cdot H_2O$

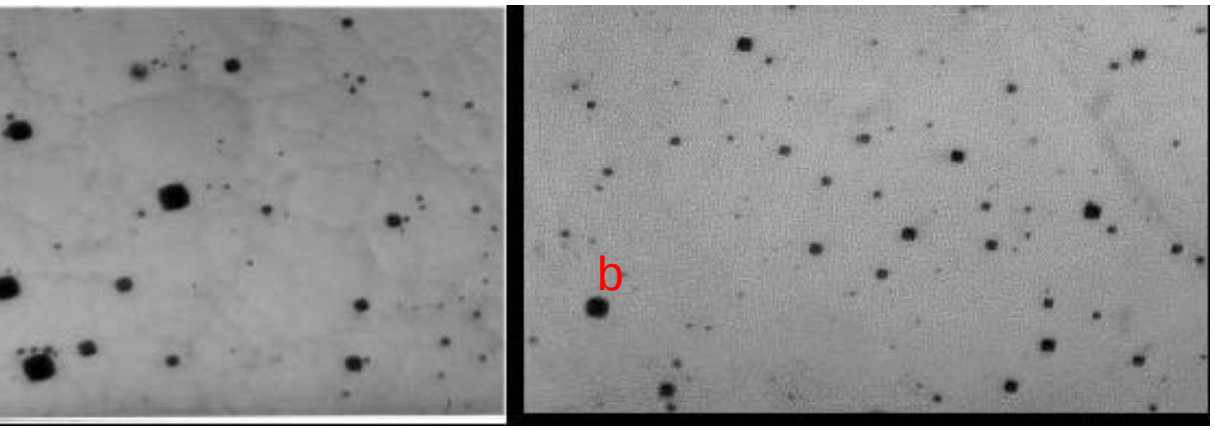

Fig.2.19. Microscop photograph of n type<100> Si membrane, (150x120 μ^2) dimension, etched in

a) 4.5M NaOH

b) 4.5M NaOH+ptert butilfenol

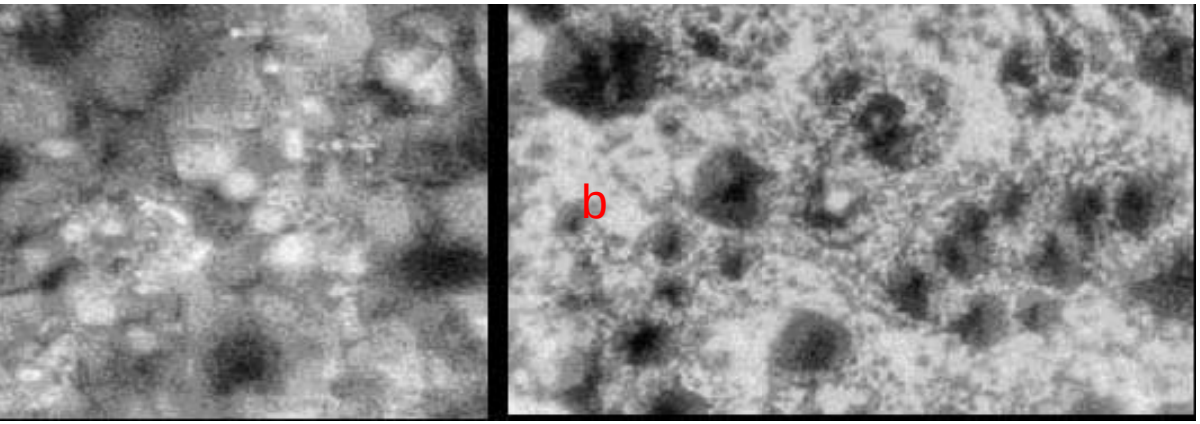

Fig.2.20. Microscop photograph of n type<100> Si membrane (150x120 μ^2) etched in a)$LiOH \cdot H_2O$ b) $LiOH \cdot H_2O$+ 10^{-4}M/l p-tert butilfenol

Fig.2.20. SEM picture of n type<100> Si

OMPARISON STUDY OF SILICON HILLOCKS FOR ANISOTROPIC IN KOH, NaOH and $LiOH \cdot H_2O$ without and with complexants added

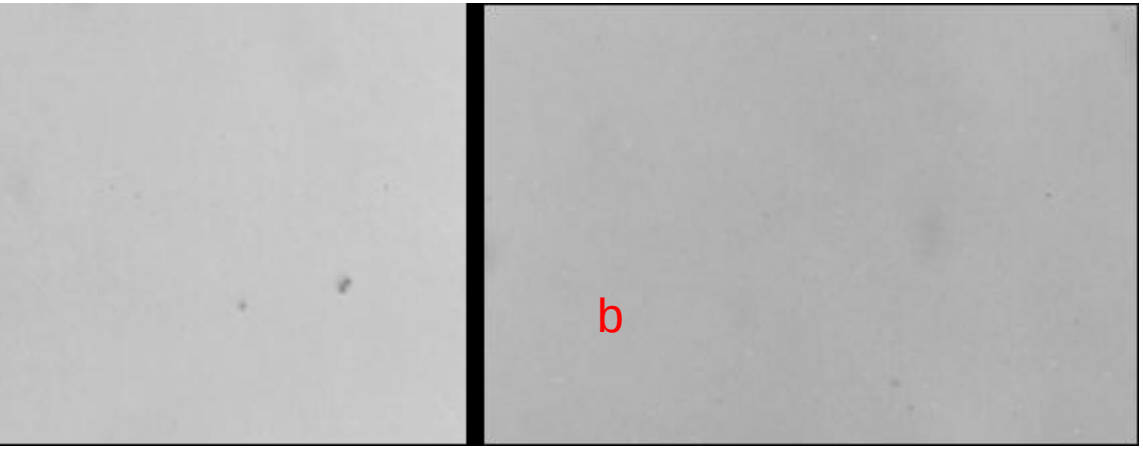

Microscop photograph of silicon surface etched in

a) 4.5M KOH,

b) 4.5 M KOH+ptert butyl phenol

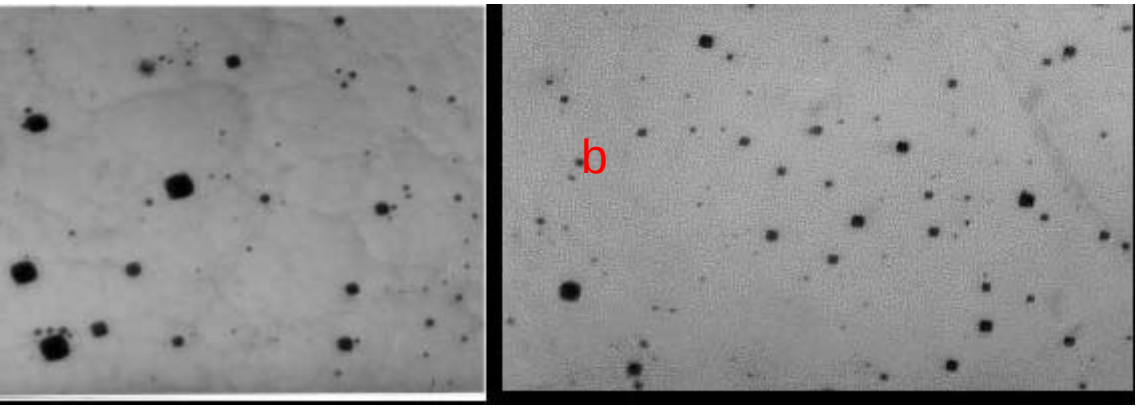

Microscop photograph of silicon surface etched in

a) 4.5M NaOH,

b) 4.5 NaOH+ptert butyl phenol

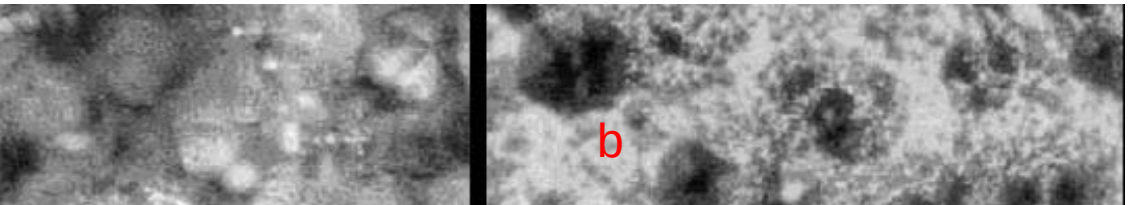

Microscop photograph of silicon surface etched in

a) 0.5M Li OH,

N OF BULK MICROMACHINED SENSORS

micromachining technology is a complex technique, offering a wide range ilities in the field of sensors and microsystems microfabrication.

Design of test structures for bulk micromachining technology characterisation

gn of test structures for characterisation of 3D silicon micromachining gy are important for:

- minimizing the number of experiments;
- optimisation and control of anisotropic etching process,
- mask materials,
- lithographic configuration,
- establishing of design rules for 3D microstructures,

DESIGN OF CONTROL AND TEST STRUCTURES

ning the structures for control and test it is necessary to know:

has a diamond cubic crystal structure. The Miller indices of the main graphic planes of silicon are <100>, <110>, and <111>

con etch rate in anisotropic solutions in the <100> direction is slightly higher e <110> direction and both are much higher than in the <111> direction

different structures can be defined in an unique process sequence, by using ask three different structures: one window which penetrates the wafer, a V- nd a square diaphragm on the back side of the wafer (Fig.2.32, for silicon 2.33 for silicon <110>)

ragm is defined by B++ doping.

> planes form (each one) an angle of $54{,}74^0$ (for silicon <100>) and the slope ngth of $54{,}74^0 \text{arctg}\sqrt{2}$

ing a diaphragm on silicon <100>

$$= W + \sqrt{2} \cdot h$$

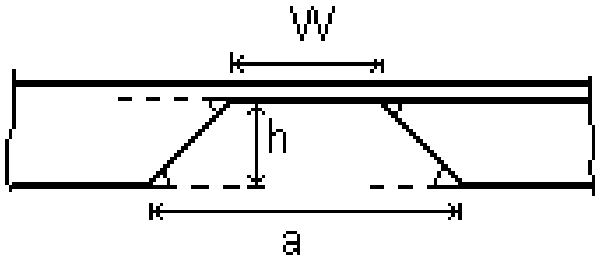

ning a V-groove on silicon <100>

idth of the V-groove is √2 x thickness of ched silicon

l = 2a = √ 2 x h

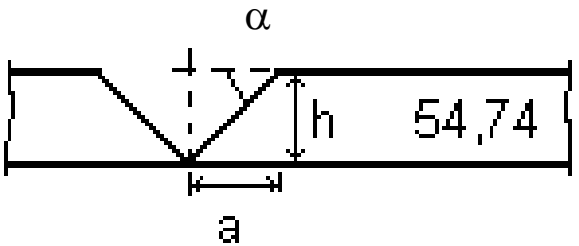

4,74° for Si <100>

CMOS TECHNOLOGY AND BULK MICROMACHINING

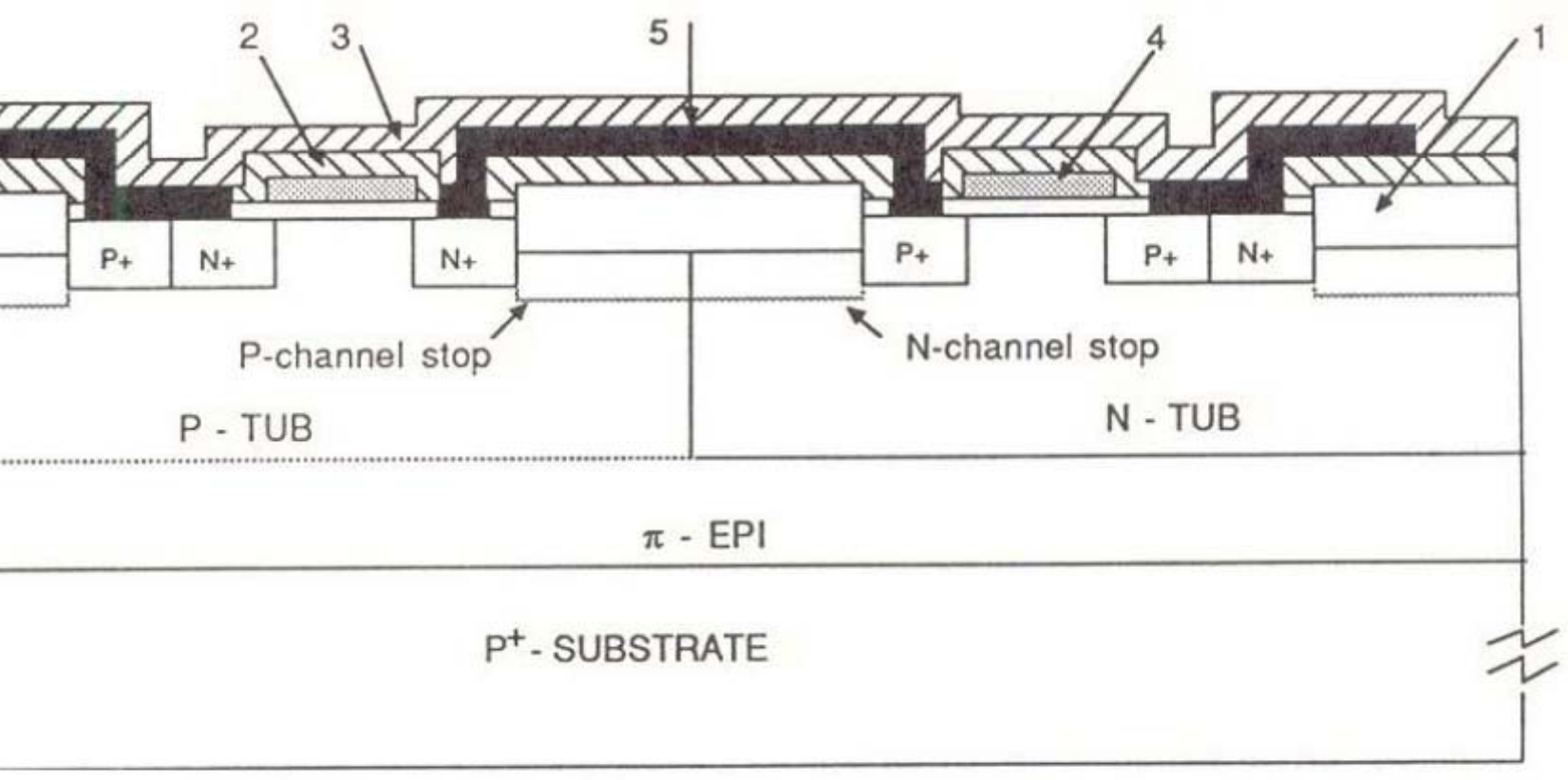

Bulk micromachining technique

Silicon wafer

Deposit Positive Photoresist

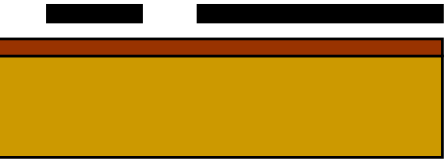

Mask

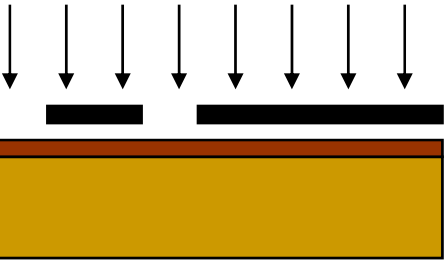

UV Light

Develop resist

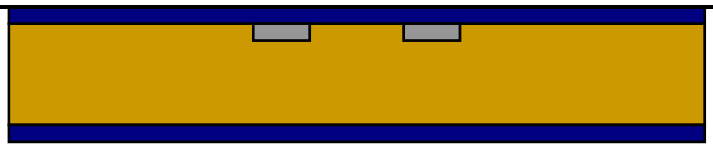

Anneal and Oxidation

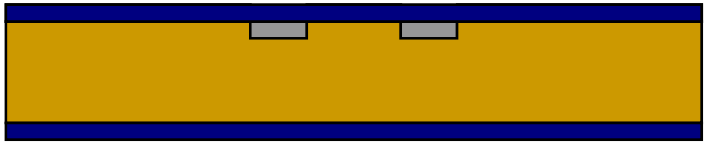

Open Contacts

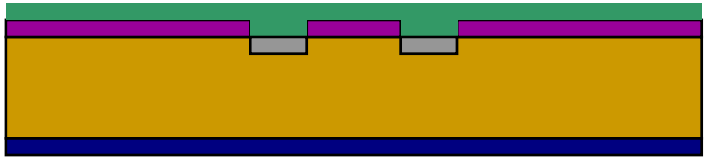

Deposit Aluminium

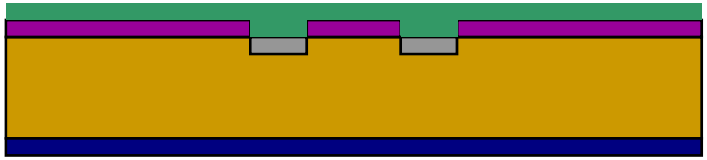

Pattern Aluminium

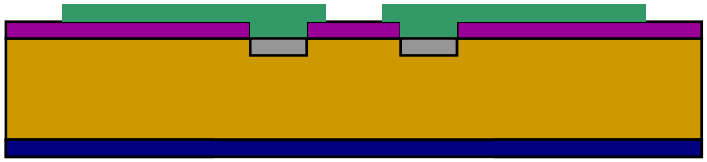

Pattern Back Oxide

PATTERNING -1

shown in Fig. 2.34. has only concave corners, which are not usually if the opening is oriented properly. This way, the truncated pyramidal pit can ed (Fig.2.35)

ORIENTATION in the<110> directions

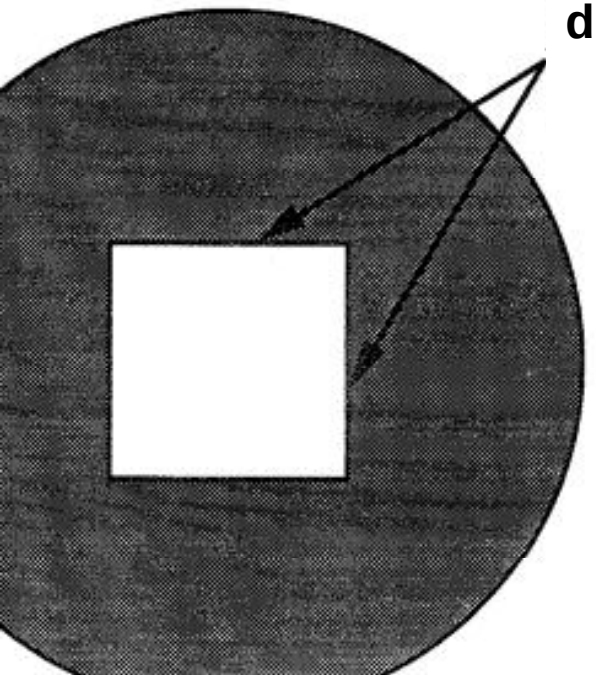

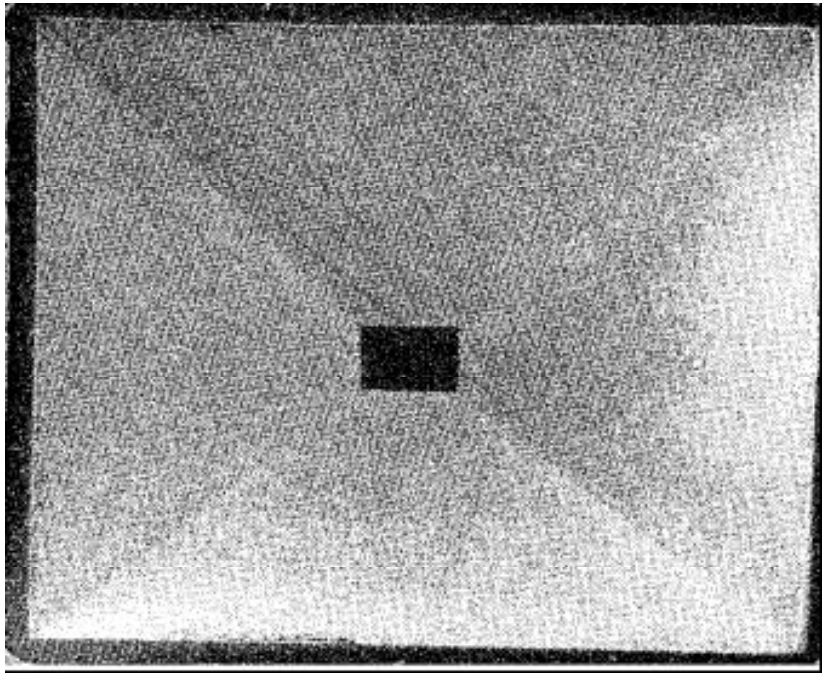

PATTERNING - 2

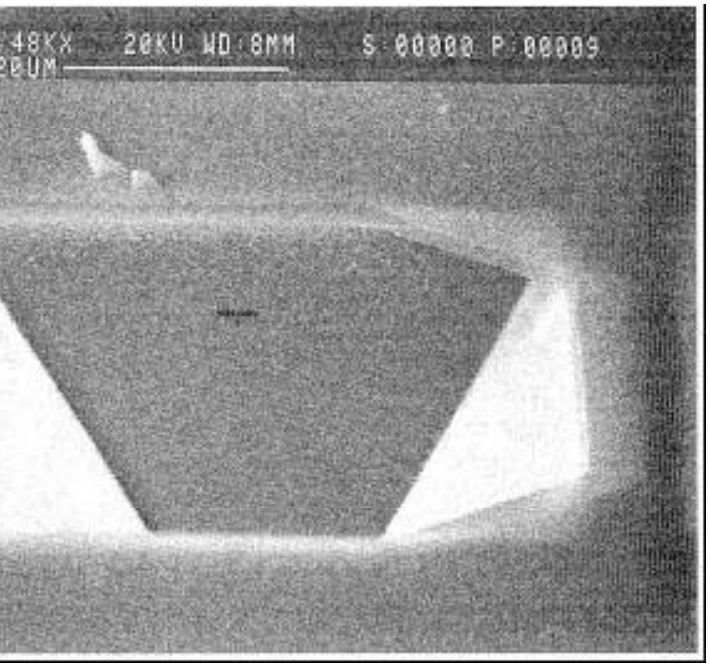

Fig.2.36. Undercuttting of improperly aligned edges. Improperly aligned edges are the corners on the right side

hip between opening, surface orientation and structure

window	Surface orientation	Structure
	<100>	Pyramidal pit or truncated pyramidal pit
	<100>	Rectangular pit (trench)

PATTERNING - 3

nd experimentally that the undercutting depend on the total etching time and nt of local surface area attacked by the etch.

a, illustrates the pattern with two convex corners and the undercutting na taking place during silicon etching, Fig.2.37 b .

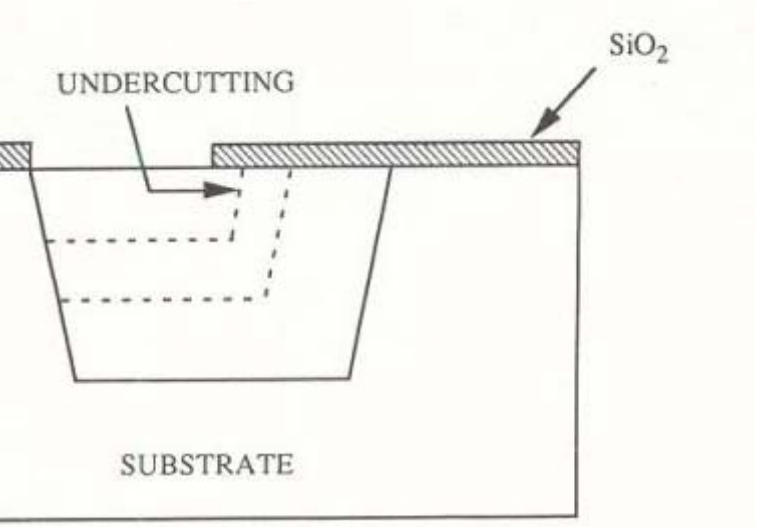

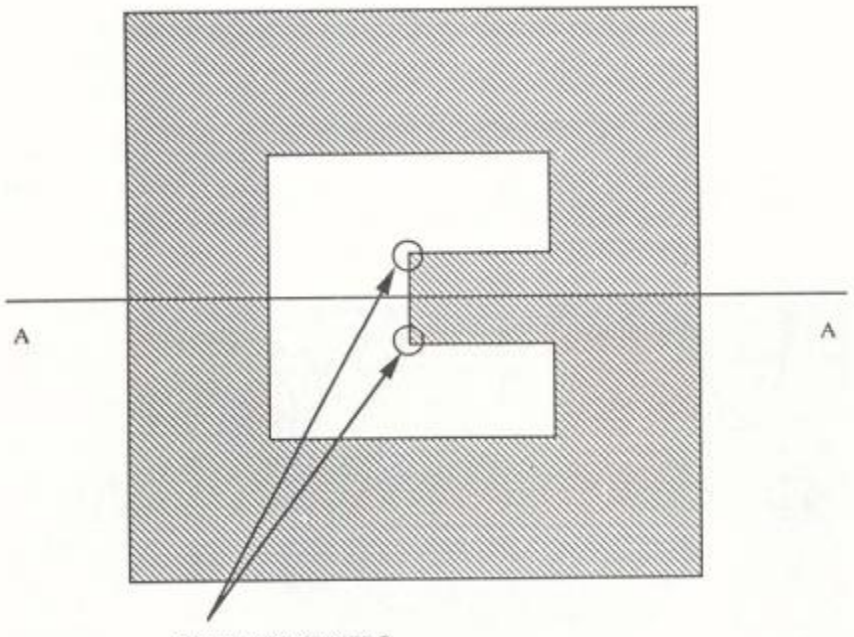

PATTERNING - 4

ral different examples of undercutting are shown in fig. 2.38-2.40

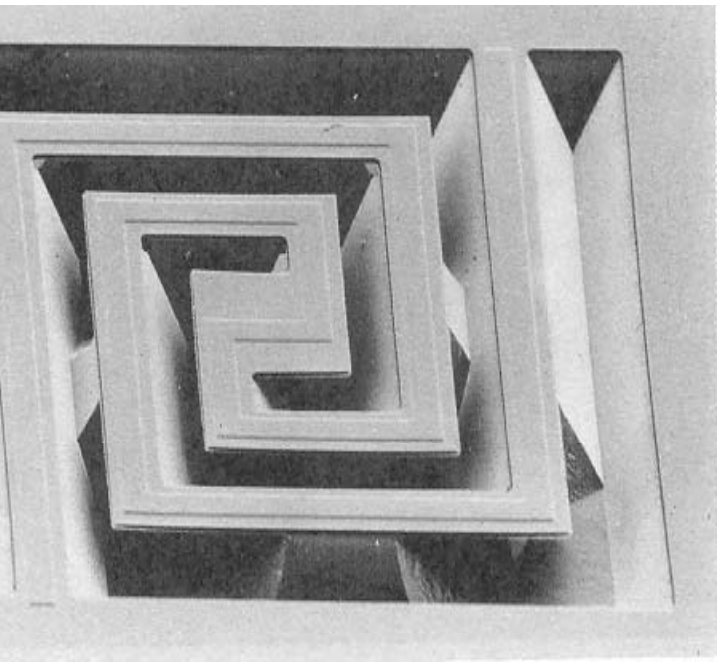

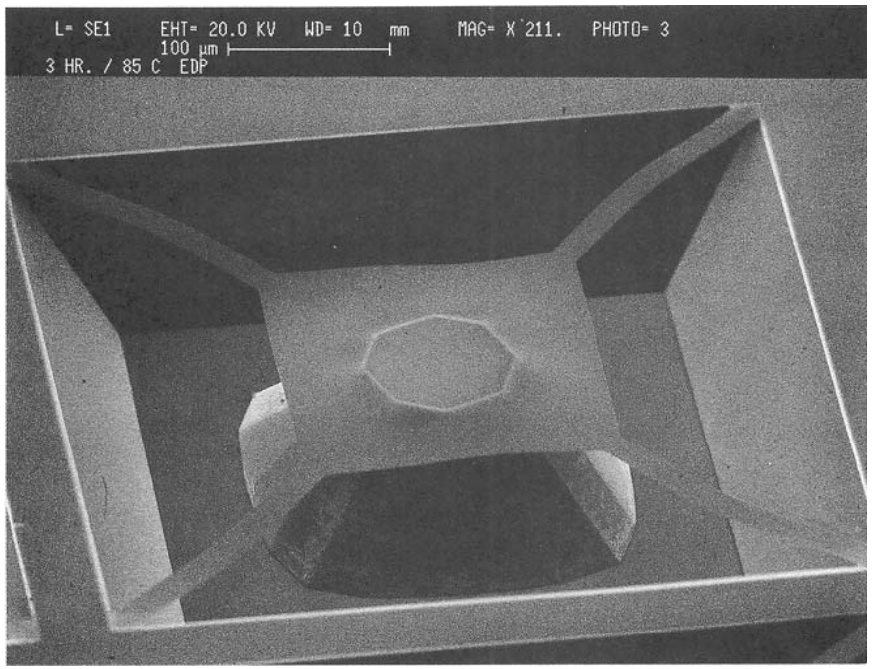

PATTERNING - 5

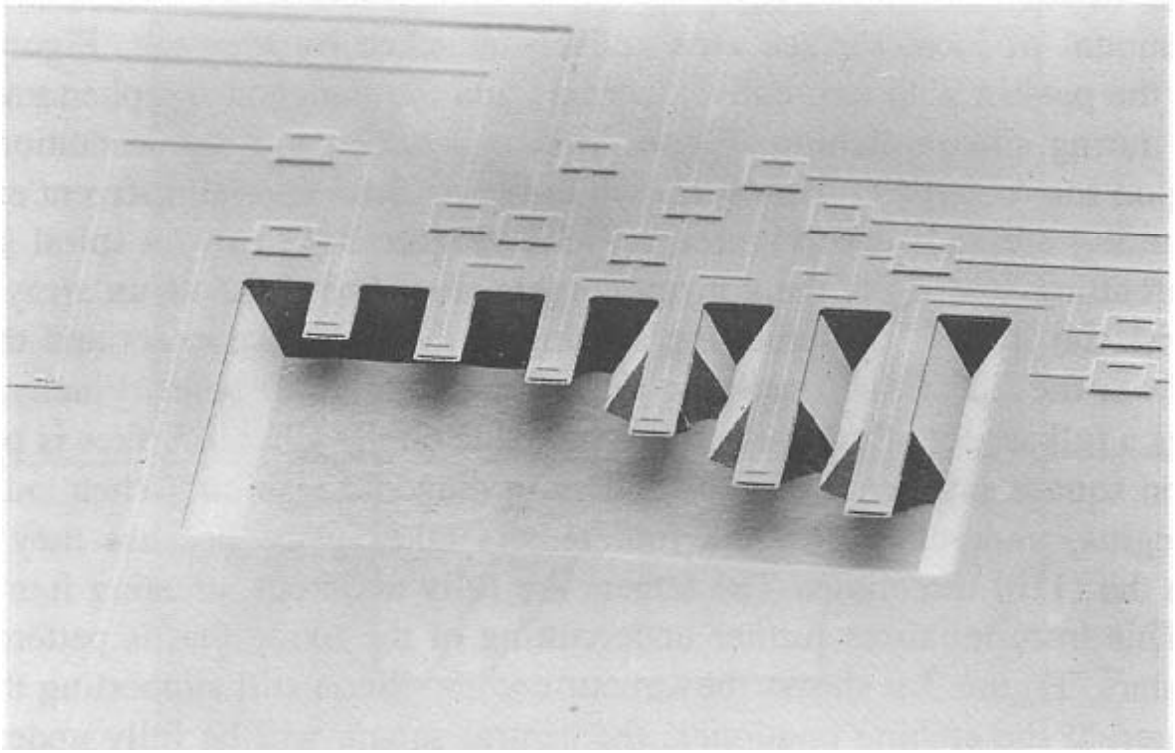

Fig.2.40. Undercutting progress in a cantilever array

PPLICATIONS AND EXAMPLES

PIEZORESISTIVE PRESSURE SENSOR

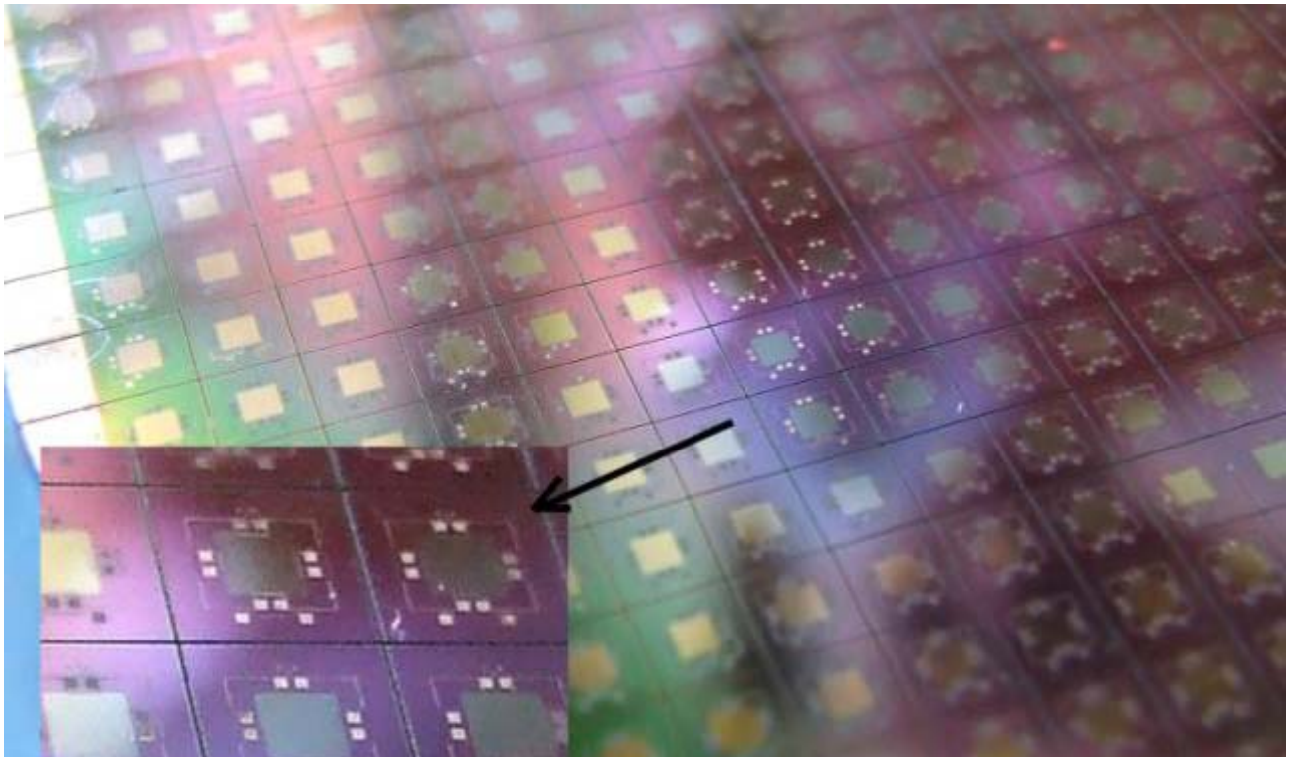

Bulk micromachining technique

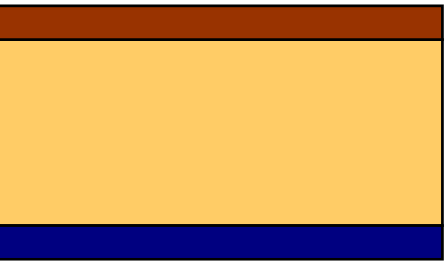

SiO_2

Silicon

Si_3N_4

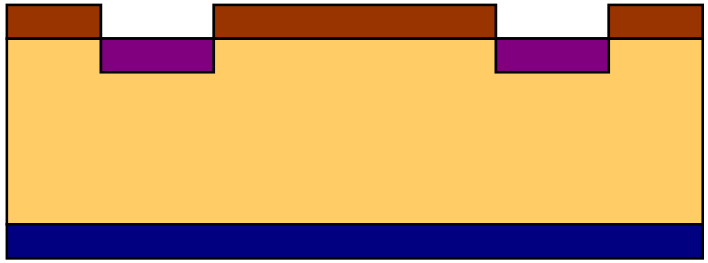

SiO_2

Piezoresistors

Silicon

Si_3N_4

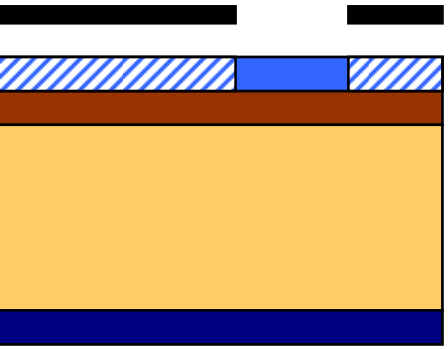

Mask

Hardened resist

SiO_2

Silicon

Si_3N_4

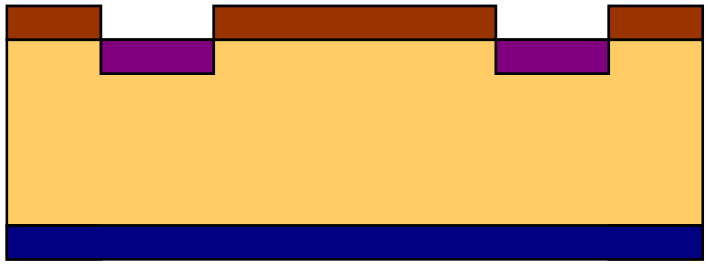

SiO_2

Piezoresistors

Silicon

Si_3N_4 – Plasma etched

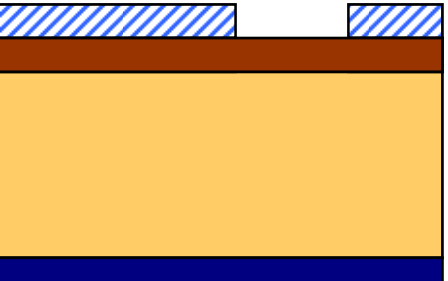

Hardened resist

SiO_2

Silicon

Si_3N_4

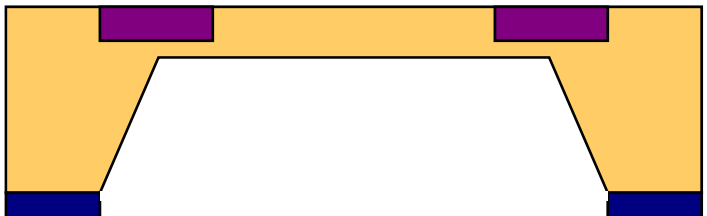

Piezoresistors

Silicon – KOH etch

Si_3N_4 – Plasma

of Science & technology
r R&D Programme
osystem Programme

Micro-capsule

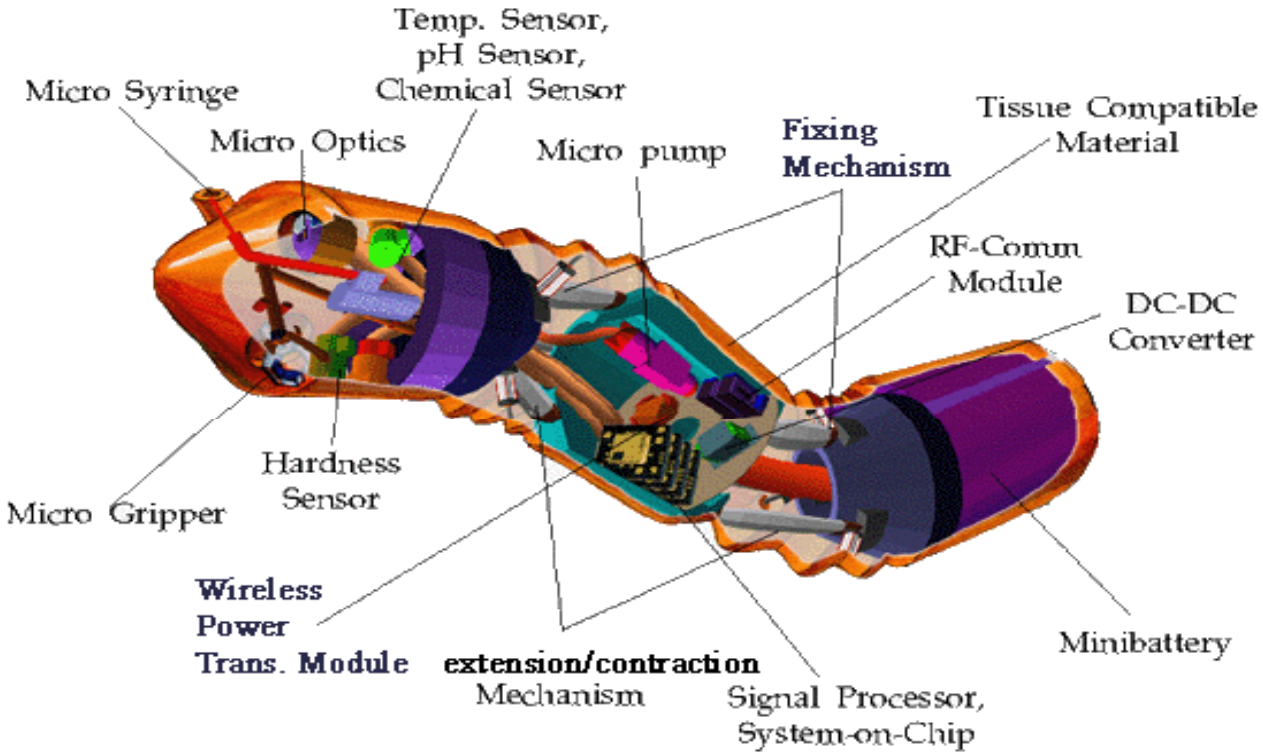

tomotive Sensors

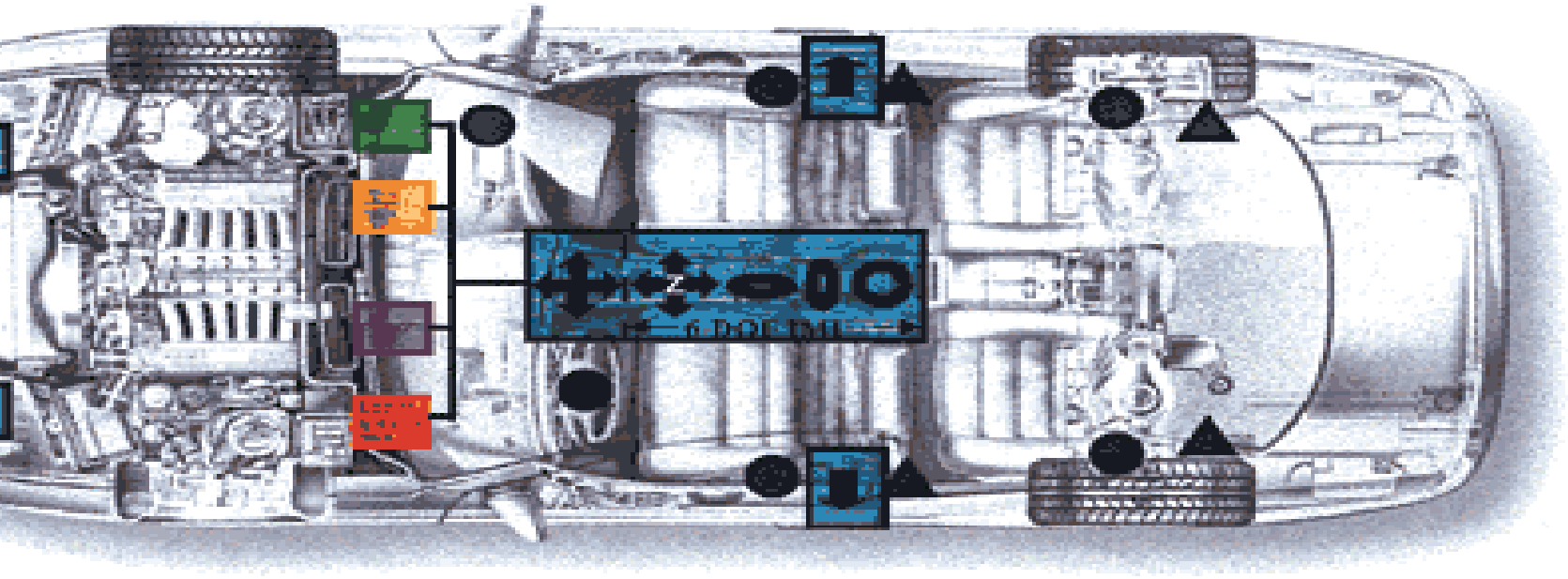

Crash Detection System

Vehicle Dynamic Control System

Navigation Information System

Body / Chassis Control System

Satellite Sensor

Airbag

Seatbelt Sensor

e of the 21st century

ns, who are thought to have built the first truly sophisticated bridges, e ages has showcased technology as well as beauty. The bridge of in. ► Cover story, 1A

the bridge

By Baltasar Korab

t

man stone-arch by Emperor with truly h as this one, as well. Mortar, as used only in s were out to fit eight.

Construction materials

Aluminum, fiberglass-encapsulated steel and high-performance, pre-cast concrete already are finding their way into bridges. The greatest promise lies in so-called advanced composites, the Space Age stuff used in everything from Stealth bomber wings to golf club shafts. Corrosion-resistant composites could replace steel cables and concrete decks, cutting weight by as much as two-thirds and cutting maintenance costs and extending bridge life by decades.

Smart paint

Lehigh University researchers have developed paint that includes tiny, dye-filled capsules. A crack under the paint would cause the surface to break, opening the paint's capsules and releasing a telltale splotch. Crews could find corrosion without close inspection.

Brain of the bridge

A computer would monitor winds, weather, temperature changes, traffic and loads, peeling paint, and internal corrosion—all data fed from sensor locations.

Epoxy binders (matrices)

Multi-directional carbon or other fibers

Self-healing construction

Epoxies, sent through tubes imbedded in bridges like human blood vessels, could repair fractures in decks and support structures.

Fracture

Epoxy tube

Cables with sensors

Environmental sensors

High winds, fog, sudden freezes, earthquakes, traffic accidents or other hazards could be detected at any spot without constant monitoring by personnel. Warning signs and traffic control devices such as lane barriers would be activated automatically.

Approach path sensors

Overweight vehicles would be detected before reaching the bridge, which would be closed automatically.

Actuators

Information is sent to bridge HQ or to the bridge itself.

Sensors

Imbedded in support cables, piers, pylons and decks, microphone- or optic fiber-like devices would sense imminent damage or collapse, then alert engineers.

Pier sensors

River cutaway

Surface heaters

Bridge operators in colder climes could eliminate the need for corrosive de-icing materials by honeycombing the deck with pipes that would heat the deck with a solution from a geothermal energy well or other source.

1994

Natchez Trace Bridge

Franklin, Tenn.

Lauded as revolutionary, elegant and economical, it carries the Natchez Trace Parkway across Route 96. It is the first and longest precast segmental arch bridge in the USA. The 1,500-foot span, designed by the Figg Engineering Group, is without the vertical members called spandrels that support the superstructure of the typical arch bridge.

eeders

roperly equipped be guided by a sensor n the roadway to a special and then sped bumper-to-bumper s the bridge without need of a driver. as on some bridges now, would be ted automatically without stopping.

Bulk micromachining technique

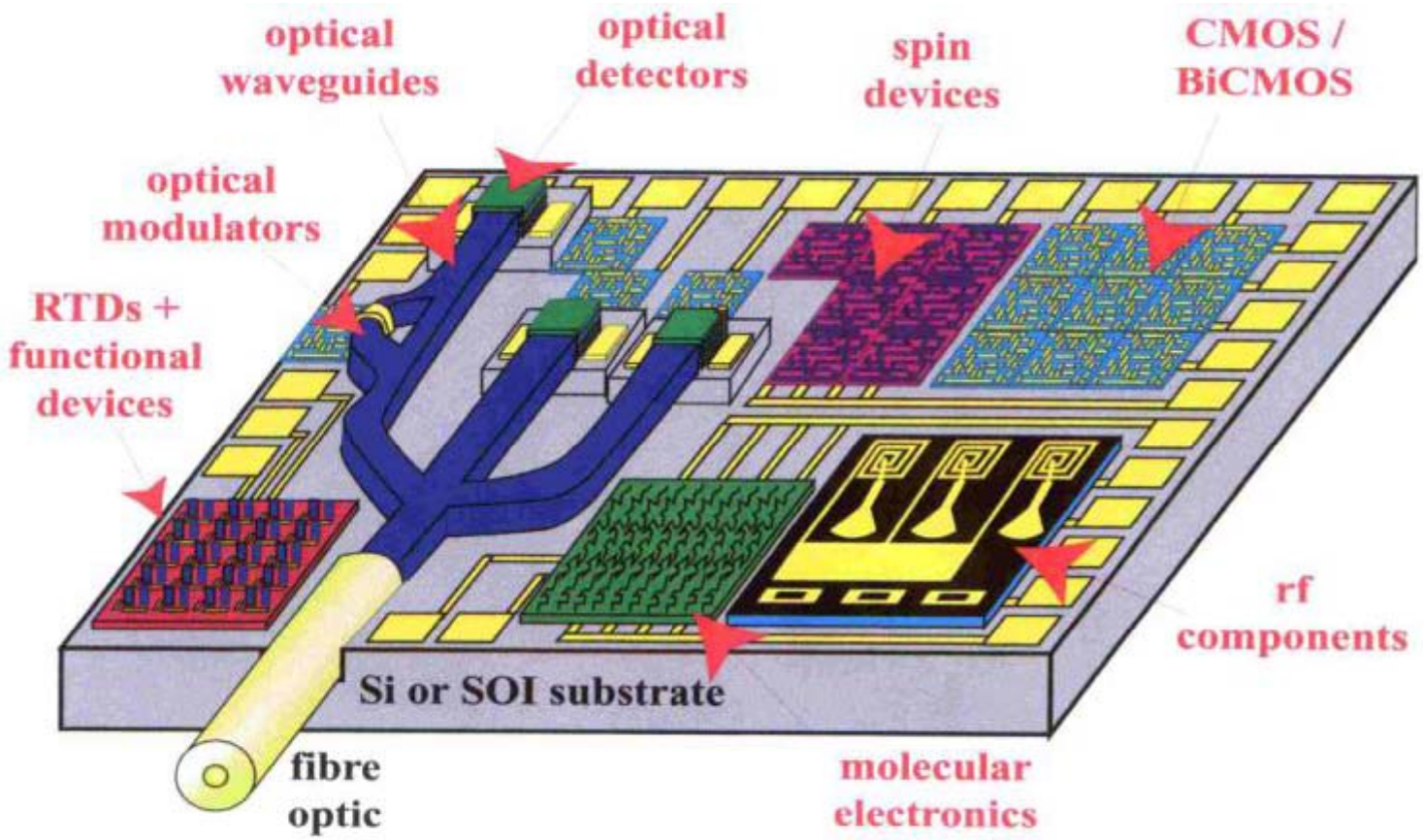

Bulk micromachining technique

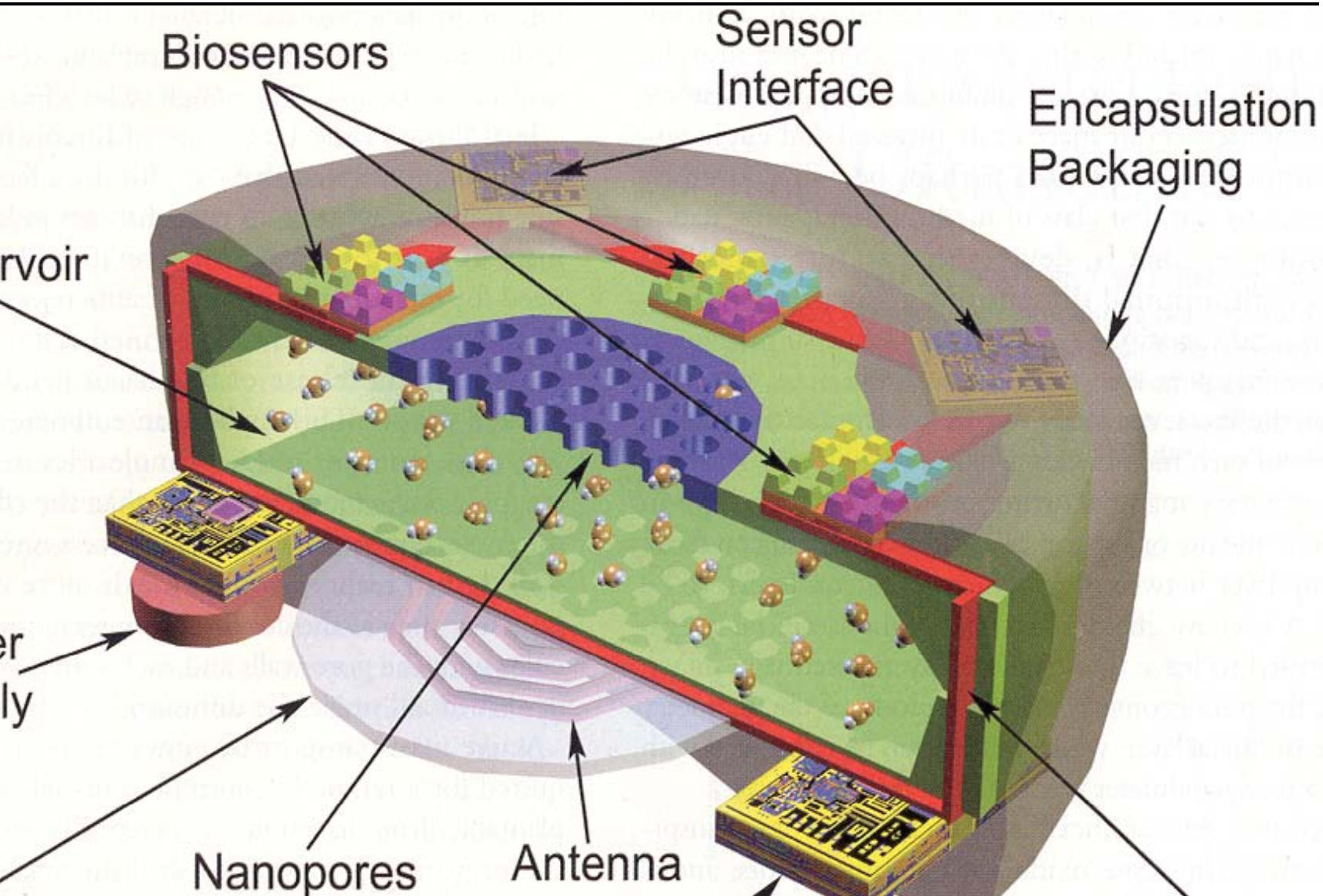

SURFACE MICROMACHINING

SURFACE MICROMACHINING TECHNOLOGY

machining technology is of realisation of 3D micro- echanical structures from deposited and patterned urface.

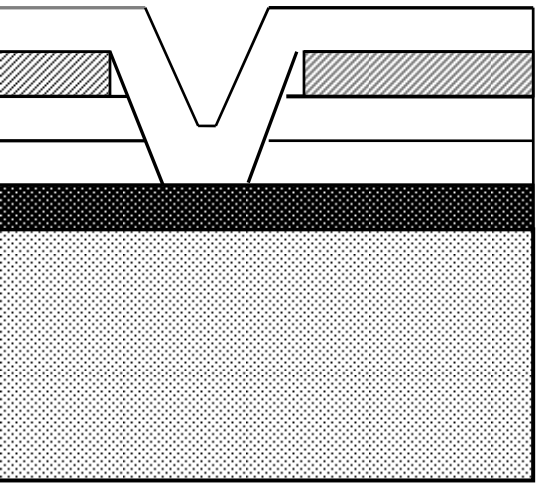

Polysilicon

Oxide undoped 1

PSG

Oxide undoped 2

Si_3N_4

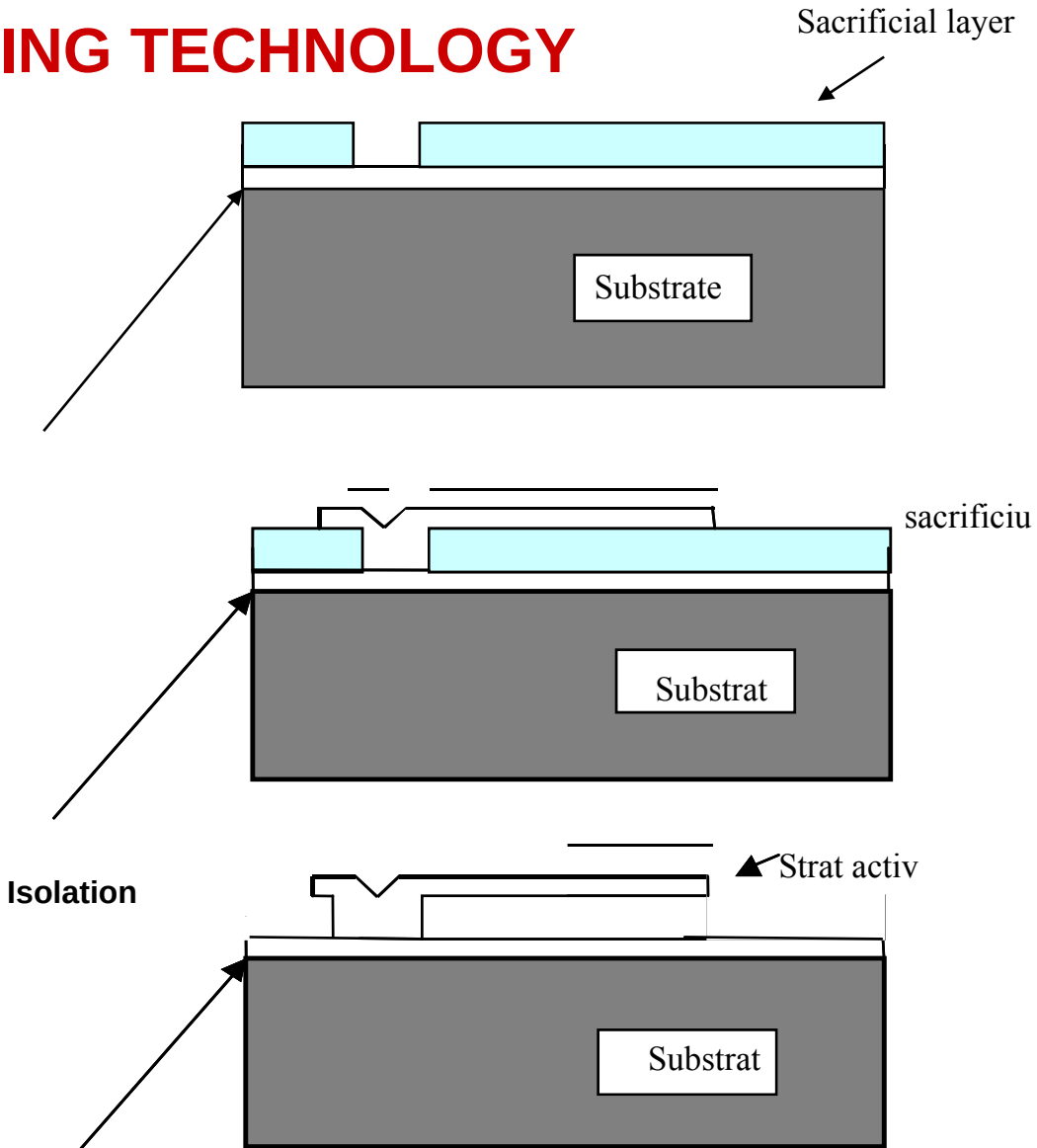

Surface micromachining technique

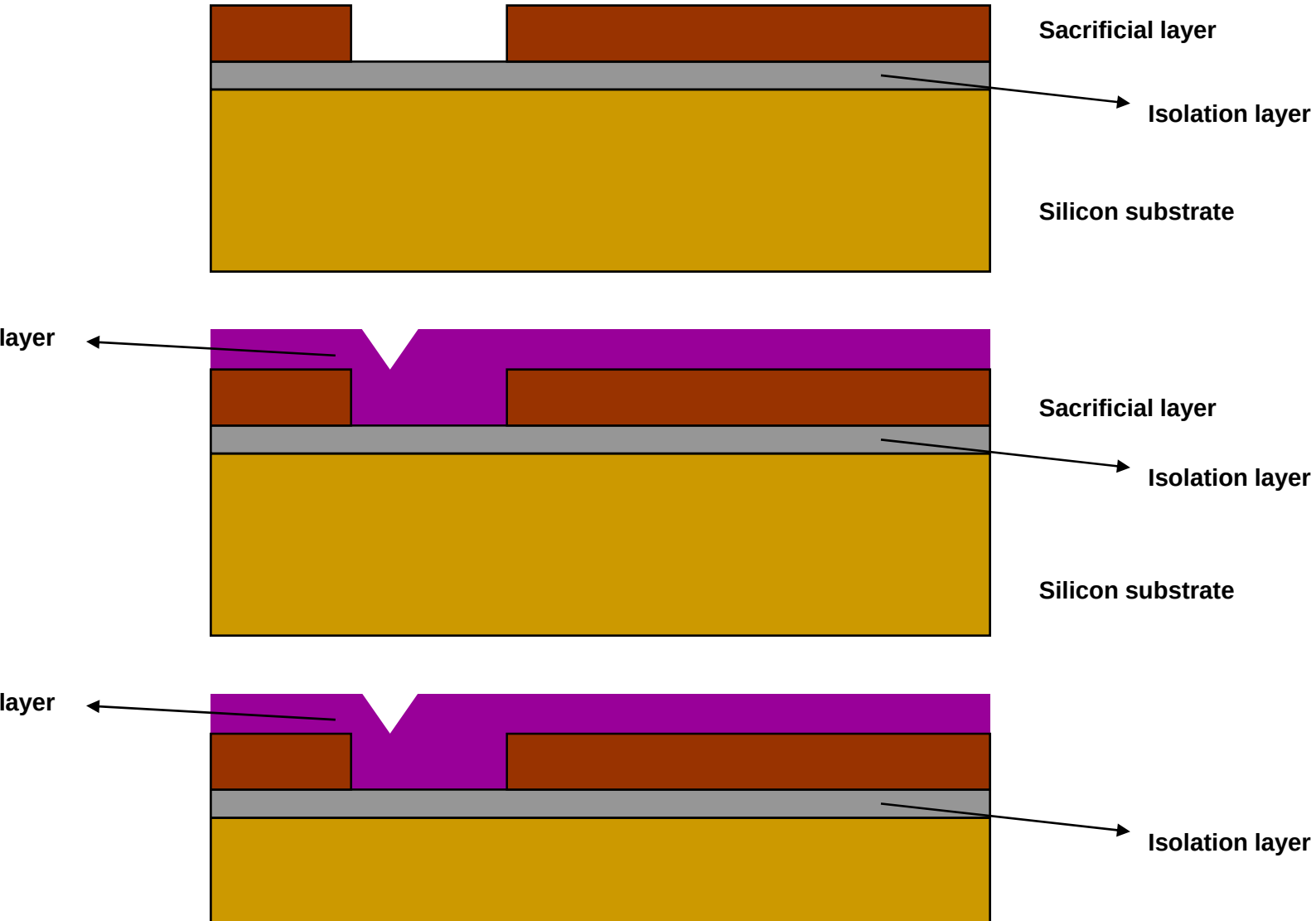

matic representation of PSG sacrificial etching mechanism

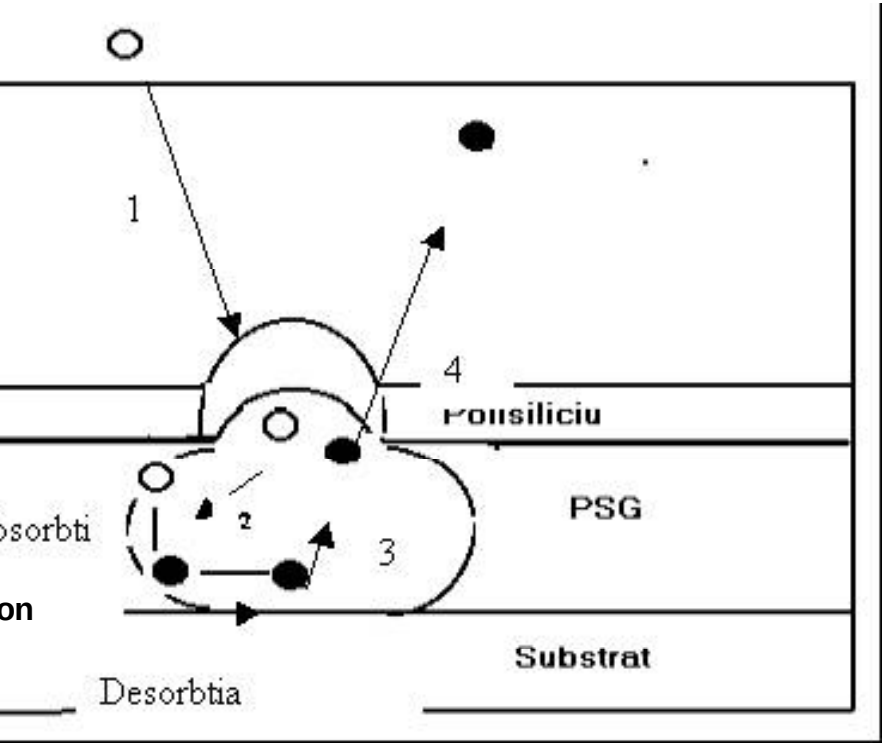

1→External Reactant Mass Transport

2→Reactant diffusion

3→Product Diffusion

4→External product Mass transport

$$\vartheta_{dif} = D_{HF}\frac{C^b - C^s}{\delta}$$ **with** D_{HF} **= diffusion length**

nnological experiments for the deposition and configuration of the layers – PSG – for surface micromachined membranes

sition and etching of PSG thin films

ne PSG layers, generally considered to be phosphor-doped silicon dioxide, are ing the APCVD method, typically at 400°C and atmospheric pressure, from silane sphine (2), in the presence of oxygen.

$$iH_4 + 2O_2 = SiO_2 + 2H_2O$$
$$PH_3 + 4O_2 = P_2O_5 + 3H_2O$$

hin SiO_2 layers and PSG oxides, with phosphorus concentrations between 3 and have been studied.

ne etching speed has been analysed, for the densified oxides, and also for the ones, using BHF-type etching solutions (fluorhydric acid with ammonium th concentrations of 1:10 and 1:15, their temperature being 35°C.

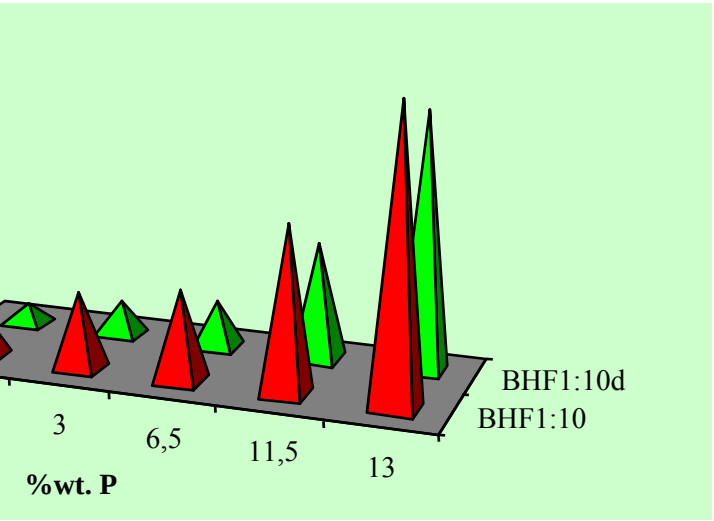

speed for deposited layers, and for deposited and
in BHF 1:10

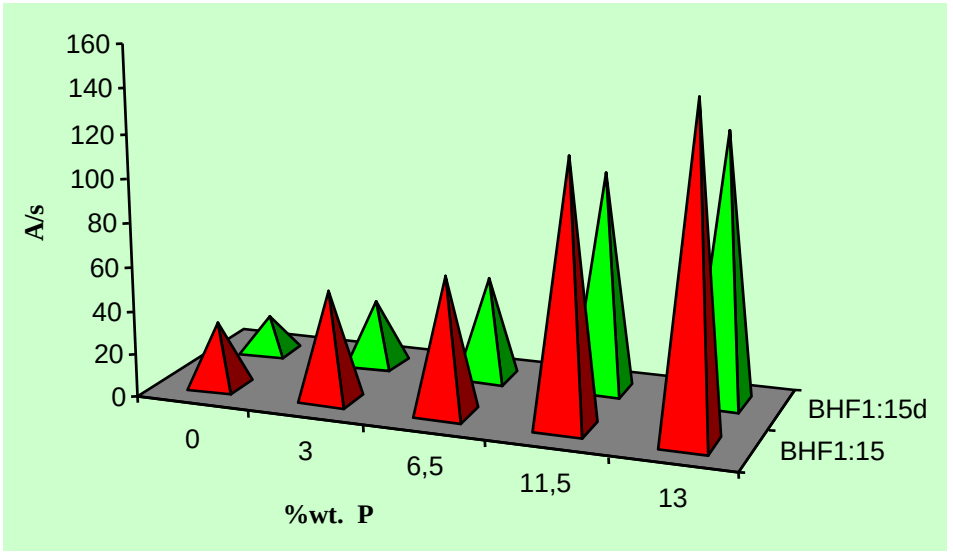

Fig.3.2. Etching speed for deposited layers, and for deposited and densified layers, in BHF 1:15

te of the doped CVD oxides (the PSG ones) and the undoped ones, in BHF 1:10 resent a nonlinear increase vs. the P concentration increase and they are higher nsified oxides than for the densified ones, except for the very high P doped e the etching mechanism is different.

se in the etching rate swith the P concentration is explained by the fact that the

. Etching of the sacrificial layer

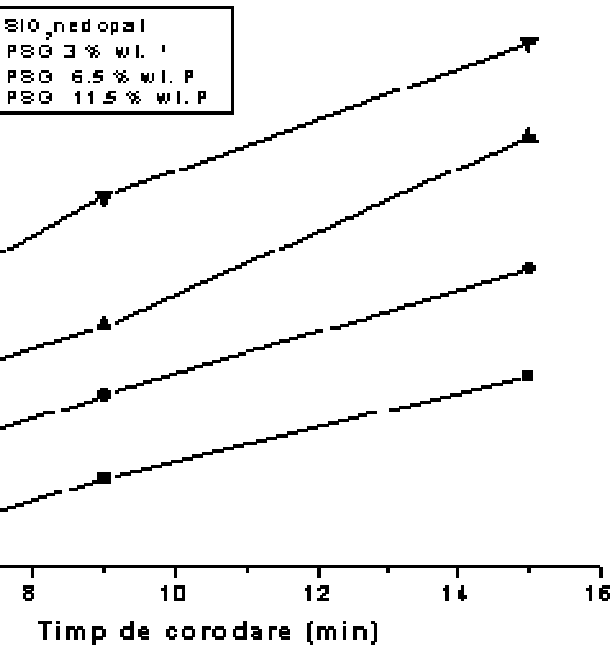

e PSG etching under the resist and
icon mask in BHF 15:1, vs. the
he SiO_2 deposited layer

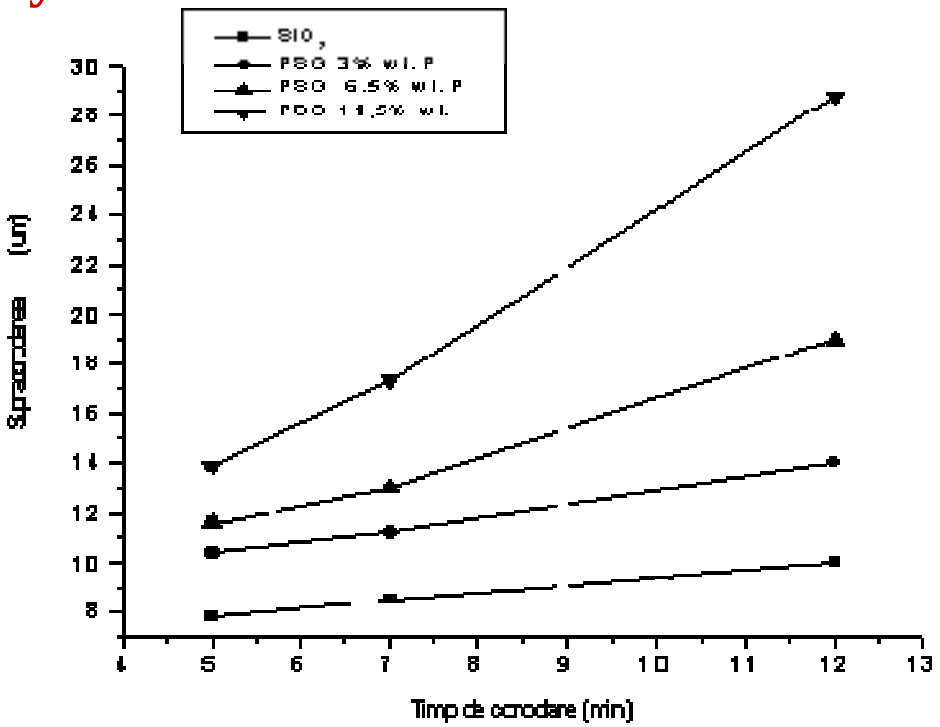

Fig.4.4. The PSG etching under the resist and the polysilicon mask in BHF 15:1, vs. the doping of the SiO_2 deposited layer

HE POLYSILICON LAYER DEPOSITION

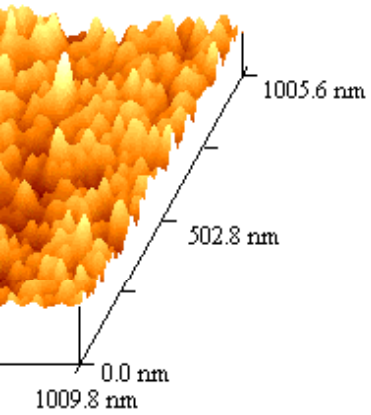

D image of the sited" layers and 53 Pa

e dimensions:
nm.
Ra): 0.6393

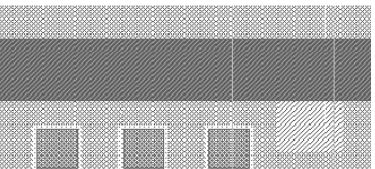

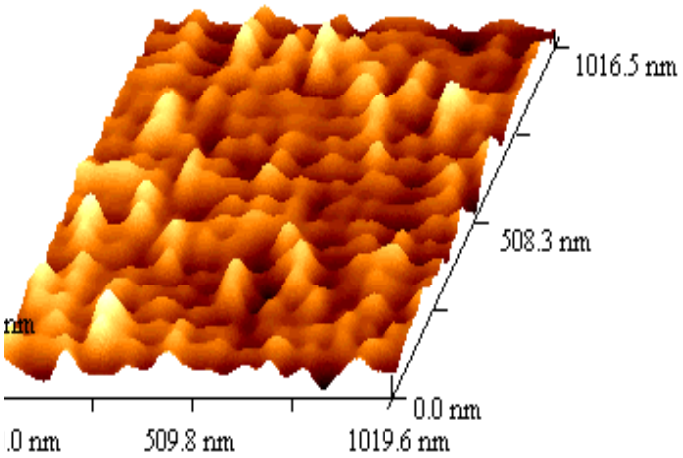

Fig. 3.8-b. AFM 3-D image of the LPCVD "as-deposited" layers surface, at 500°C and 100 Pa pressure.

The scanned surface dimensions:
1009.804 x 1005.637 nm.
Medium rugosity (Ra): 1.0387 nm.

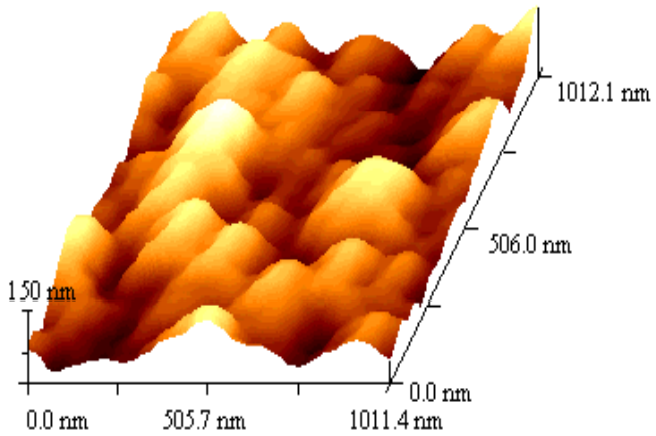

Fig. 3.9-a. AFM 3-D image of the LPCVD "as-deposited" layers surface, at 615°C and 20 Pa pressure.

The scanned surface dimensions:
1011.4 x 1012.1 nm.
Medium rugosity (Ra): 20.2348 nm.

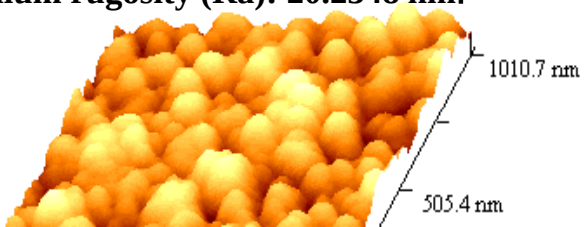

Fig. 3.9-b. AFM 3-D image of the LPCVD "as-deposited" layers surface, at 615°C and 100 Pa

sonant gas sensors surface micromachined

The resonant gas sensor
of a resonant polysilicon
ge and the measurement
o pick up the resonance
of the bridge. By coating
with sensor active material
ble to use these devices as
itive gas sensor

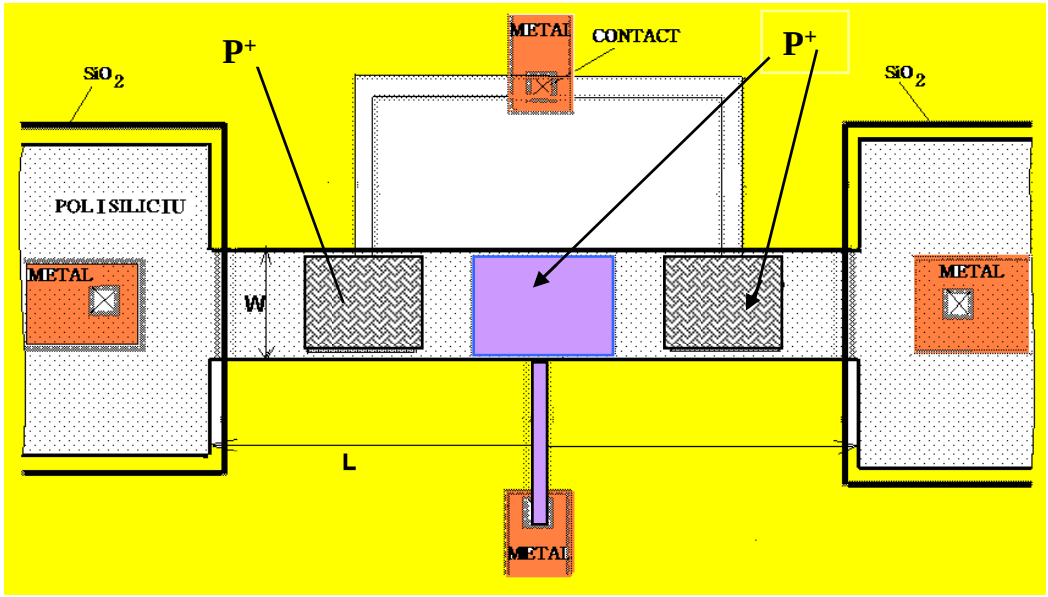

Layout of a resonant sensor: microbridge with excitation-detection electrodes

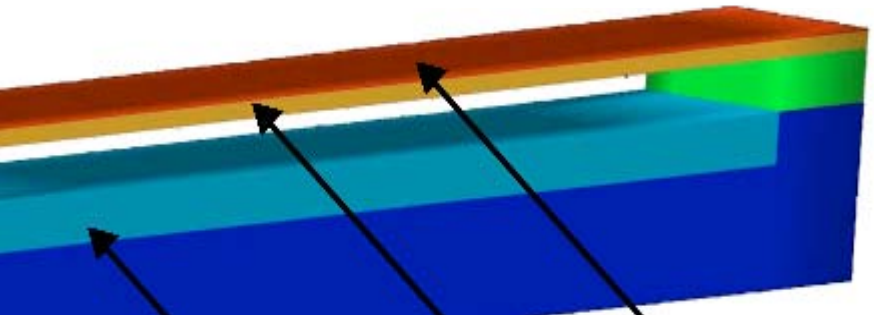

sonant gas sensors -2

Surface micromachining technique

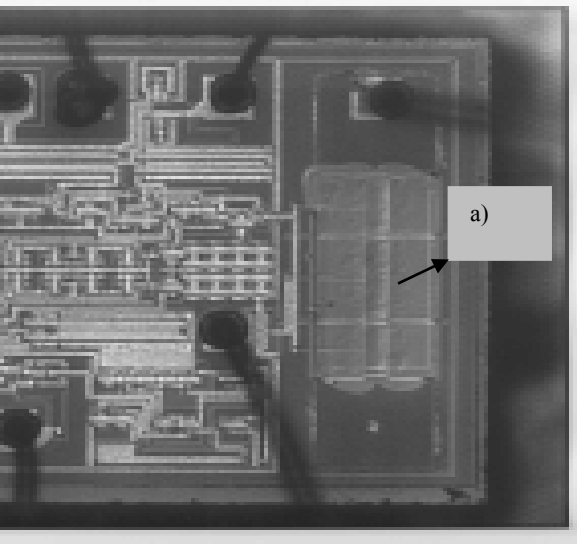

Sensor chip top view: a)bridge; b) electronics

The polysilicon microbridge is 1μm thickness. The polysilicon deposition for the bridge was realised by LPCVD, followed by lithographic configuration and planar plasma (CF_4+O_2) etching. The sacrificial oxide was then removed in BHF 10:1,

electronic circuits for excitation - detection are integrated on the same chip the microbridge, having the main aim to amplify the small current (pA) ed by the variable capacitors from detection way.

the microresonator and the excitation-detection circuits are processed on e single-crystal silicon. The technological steps for processing a double- d clamped polysilicon bridge with electronics on the same chip are based on S technology.

cterization

idge oscillation was observed under the electronic microscope SEM (Fig.5.14 tical microscope by applying an AC voltage to the drive electrode (pads 1,2 Fig.5.11). Therefore, we can conclude that the microbridge was released. This can be used on the wafer or on the encapsulated structures (fig.5.15) to nate between released and unreleased microbridges.

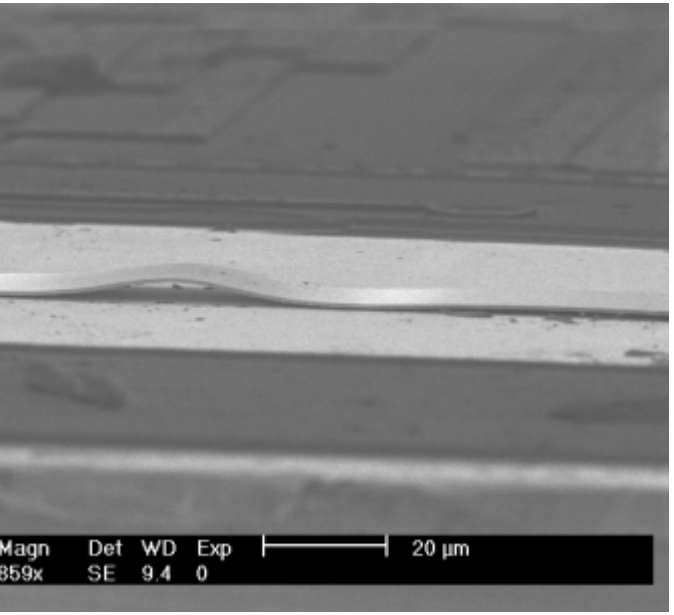

A. SEM of a polysilicon

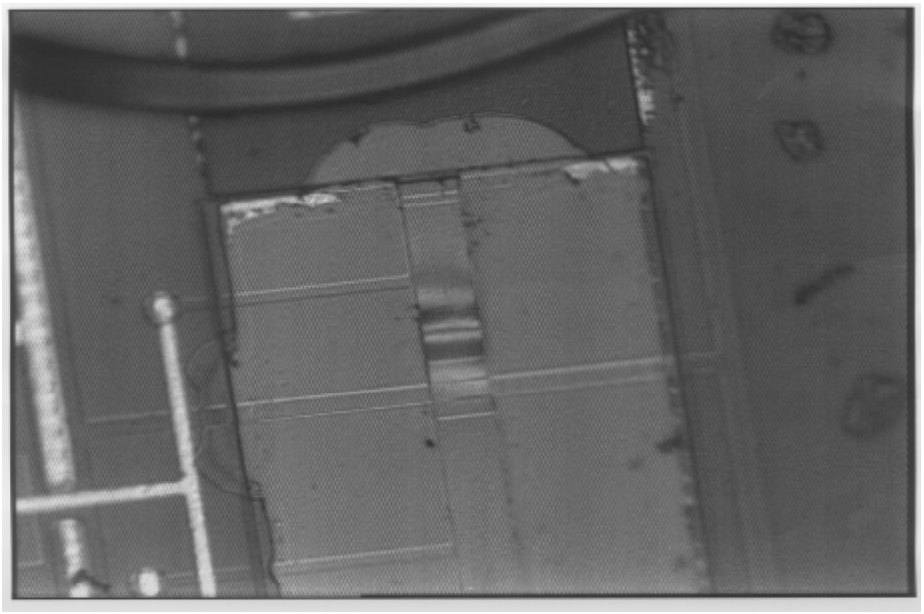

Fig. 5.14.B. Vibration of the silicon microbridge

Surface micromachining technique

TEGRATED GAS MICROSENSOR WITH ICATIONS IN ENVIRONMENT MONITORING

ERISTICS :

- gases (NOx, CO, H_2S) from media
- nsions - chip area: 1,4x1,5 mm^2,
- electronic circuits
- the same chip with the sensor
- factor: 1.000 in air, 20.000 in vacuum
- measurement: ppm ÷ hundred ppm,
- equency range: tens kHz÷MHz

SEM picture of a polysilicon microbridge (400x30 μm^2) in vibration

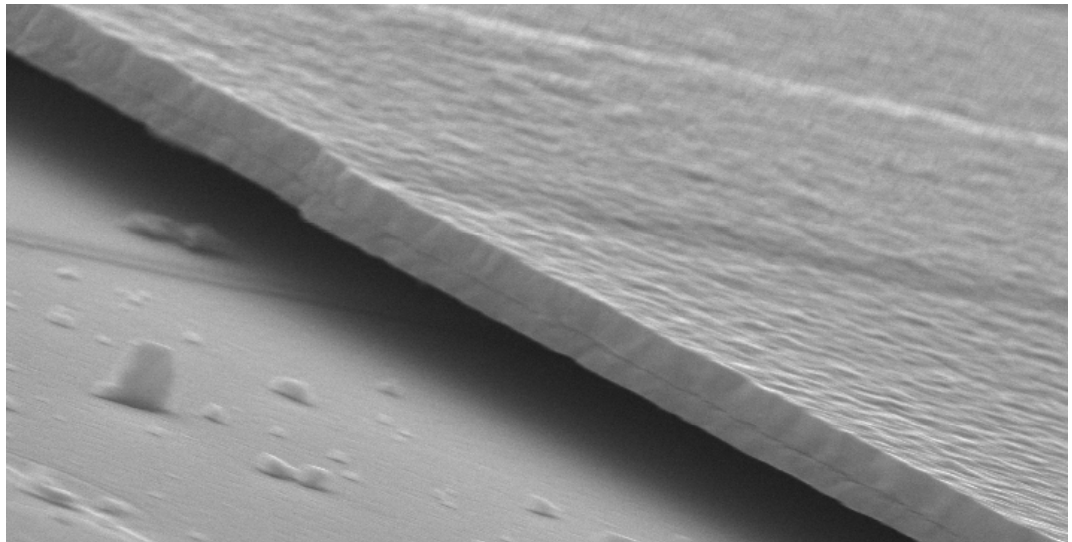

CAPACITIVE PRESSURE MICROSENSOR

ve sensors convert a change in
d into a change of capacitance
capacitor consist basically of
rode separated by a dielectric
citance change can be used
motion of one of the two
s with respect to the other
or by the change in the
between two fixed electrodes.
electrode movement is not
r if the capacitance change is
y deflection of part of the
then the capacitance change
calculated by integrating over
deformed dielectric space:

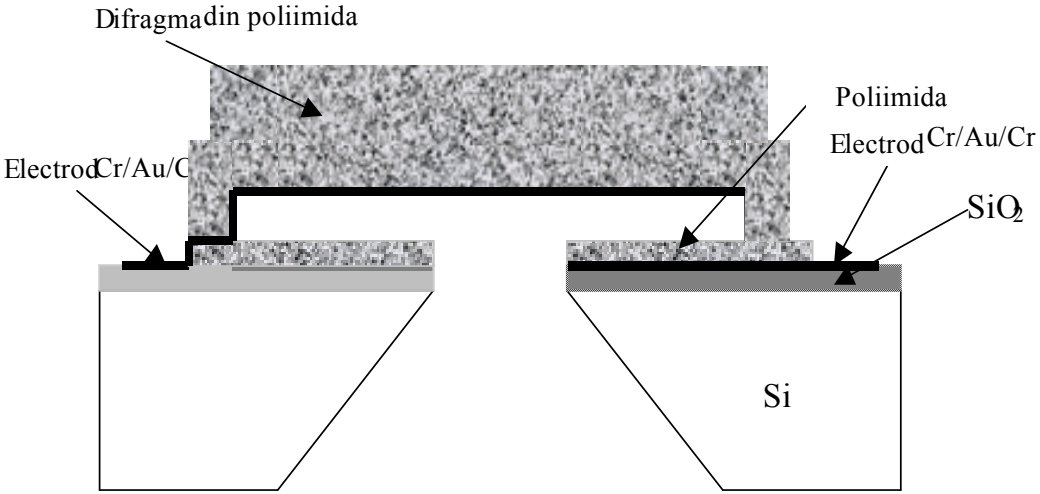

Cross section of the capacitive pressure microsensor

$$\Delta C = C_0 - \iint \frac{\varepsilon}{d - W(x, y)} dxdy$$

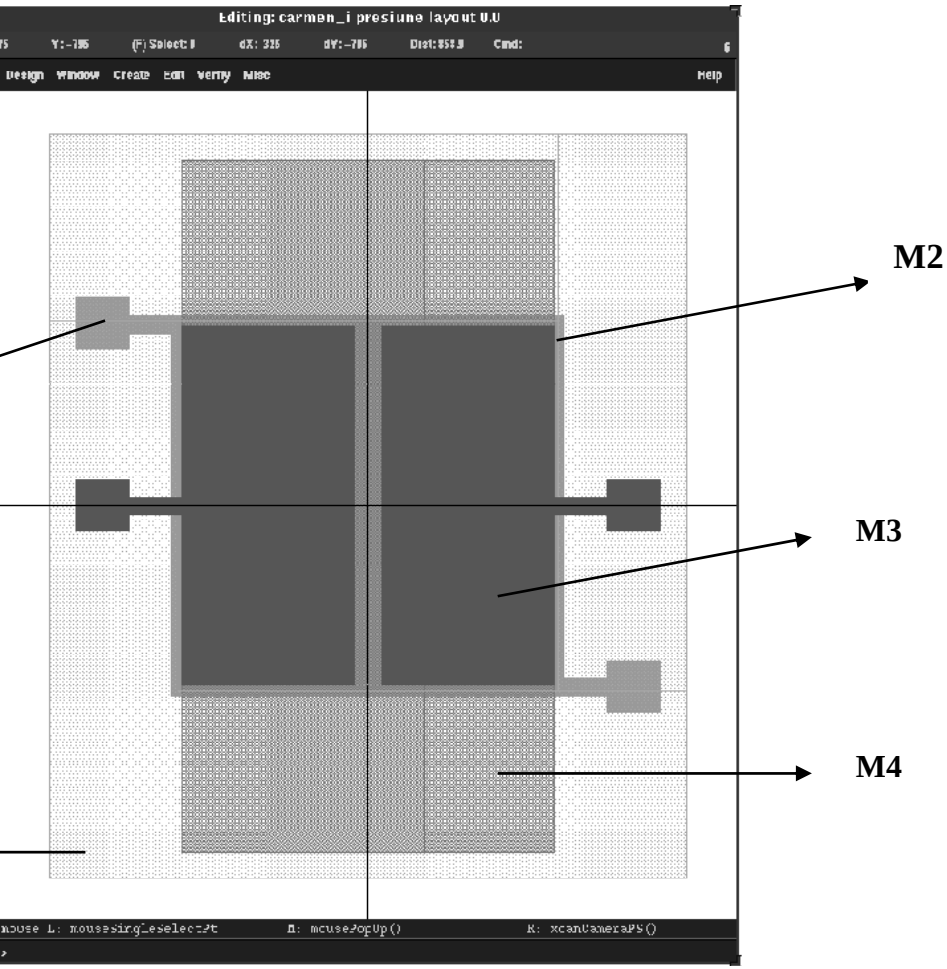

Layout of the capacitive pressure sensor

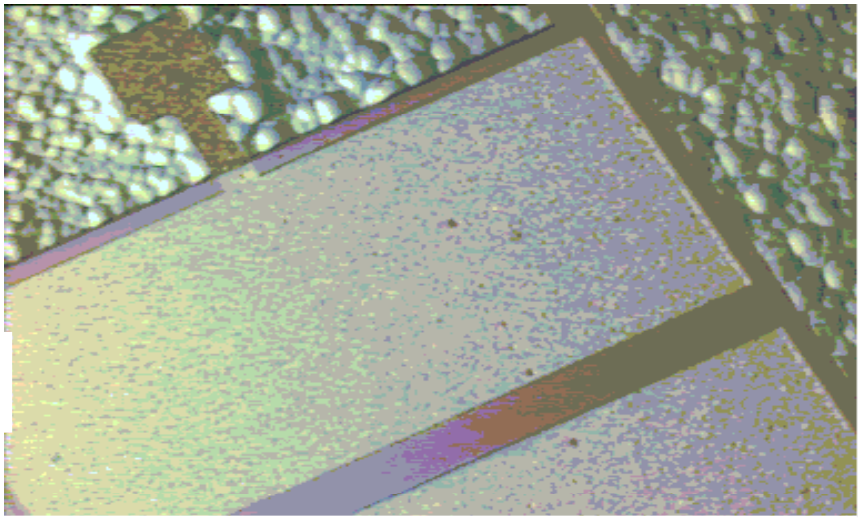

Fig.4.12. Microscopy photograph of the capacitive sensor

- **One of the electrodes of the variable capacitor is deposited on the silicon surface and is a sandwich of Cr/Au/Cr (M1)**
- **A sacrificial layer is deposited and patterned M2**
- **The second electrode Cr/Au/Cr + a polyimide membrane are deposited and patterned in two different steps M3, M4**
- **PSG is used as sacrificial layer**

acitive pressure sensor

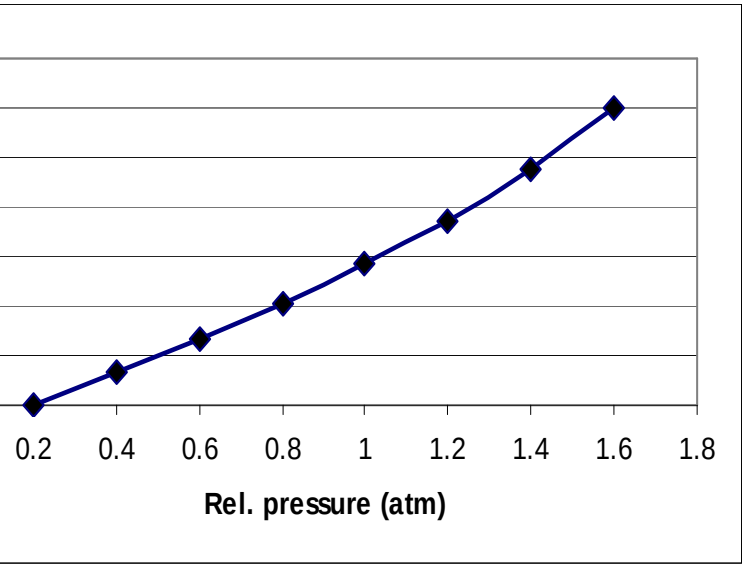

Relative capacitance change vs. applied differential pressure

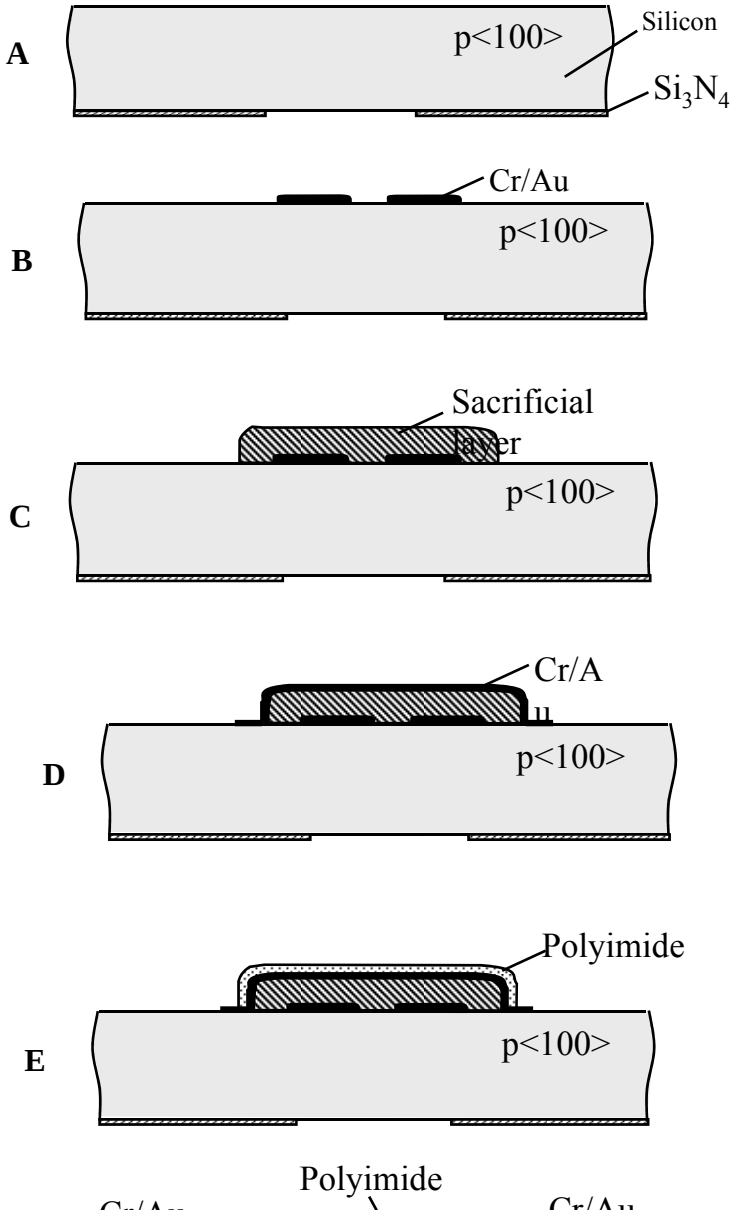

Cantilever Sensor Applications

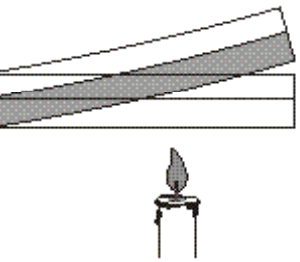

ture sensor

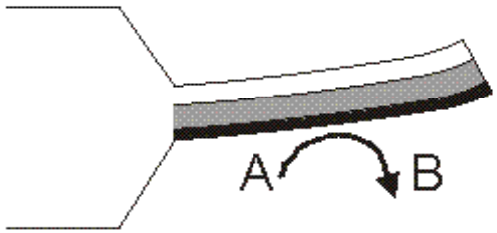

catalytical reaction

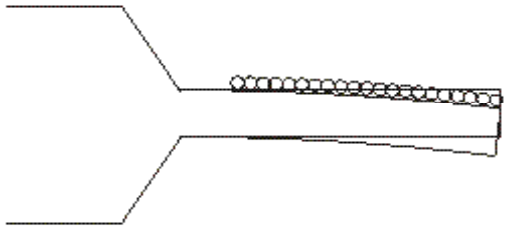

chemical sensor

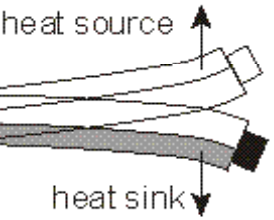

rimeter

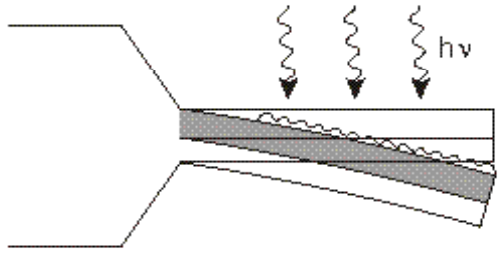

photothermal spectroscopy

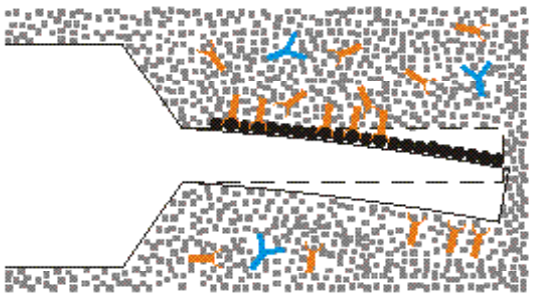

biochemical sensor

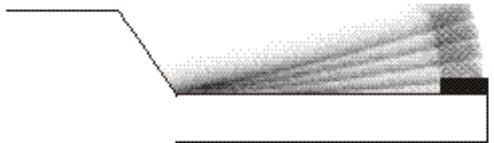

NOSE – Operation principle

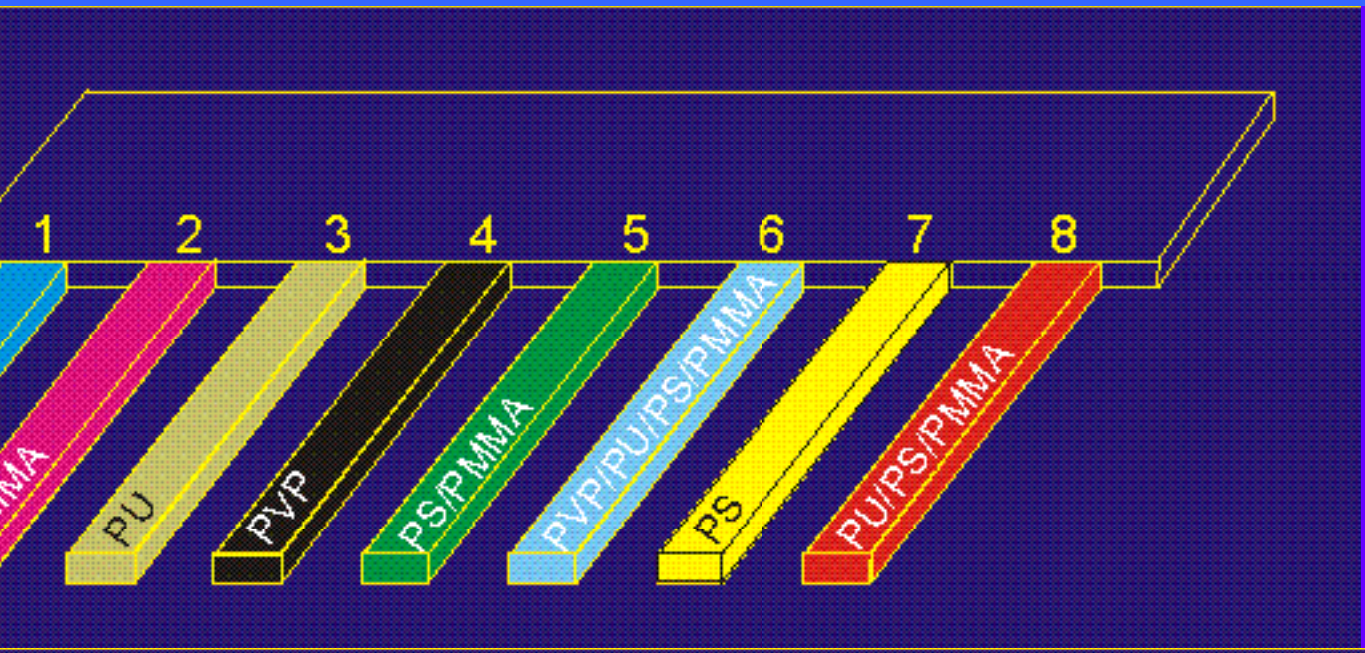

Eight cantilevers functionalized with eight different polymers or blends

on mechanism:

r layer

vered Si cantilever

Recognizing Whisky

etwork
sets
on sets

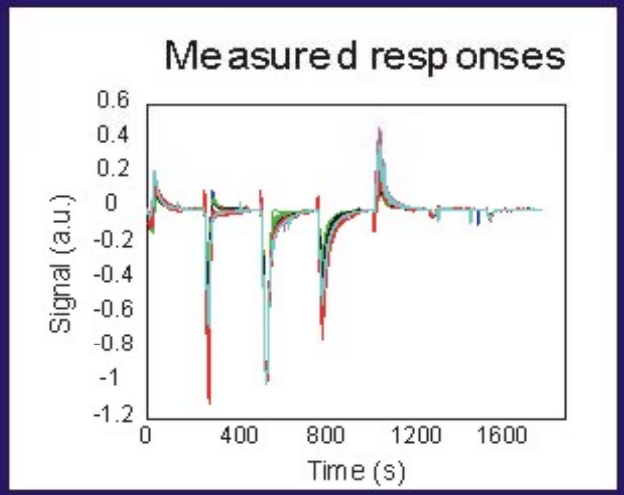

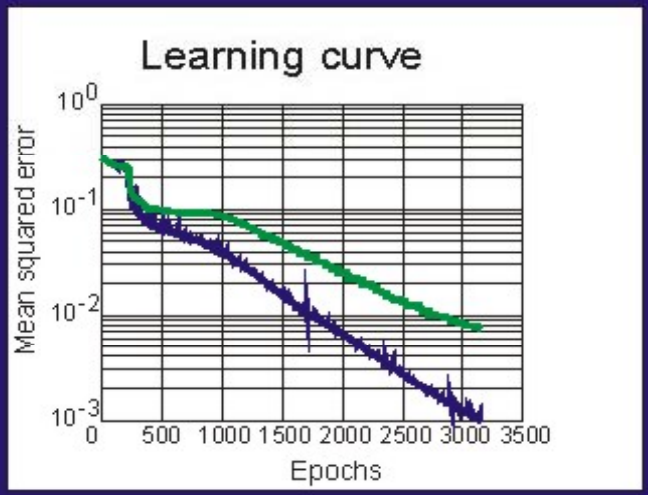

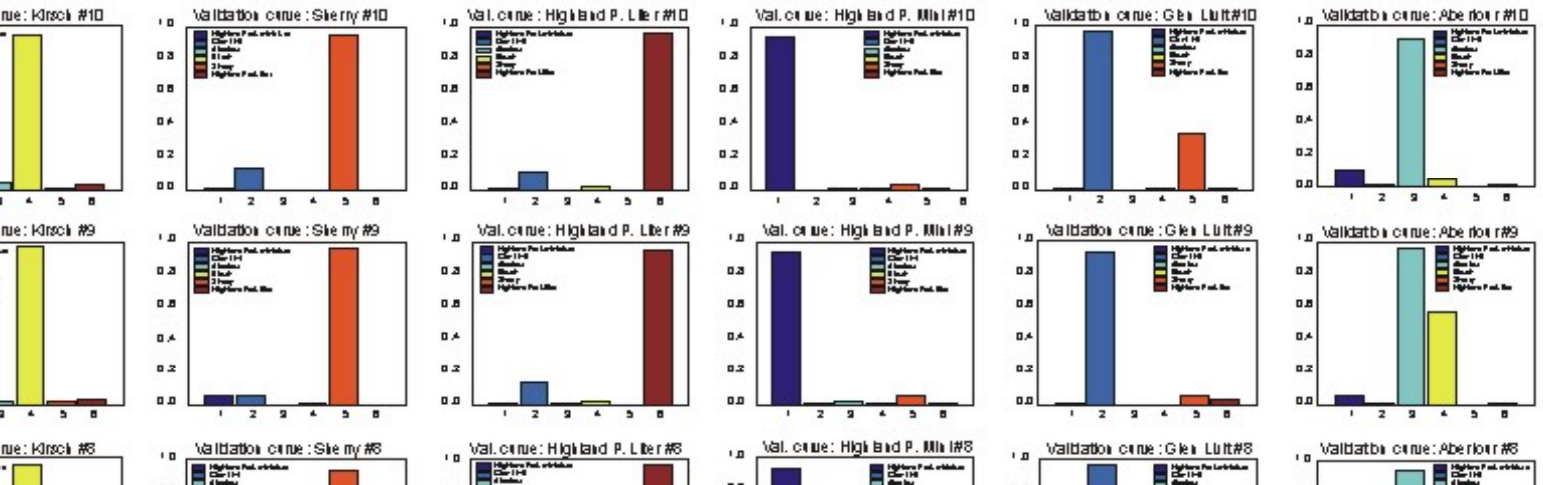

tilever Bending by Oligonucleotide Hybridization

base sequence on

Hybridization with matching complementary strands bends cantilevers

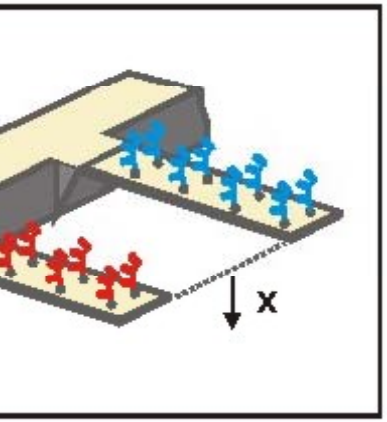

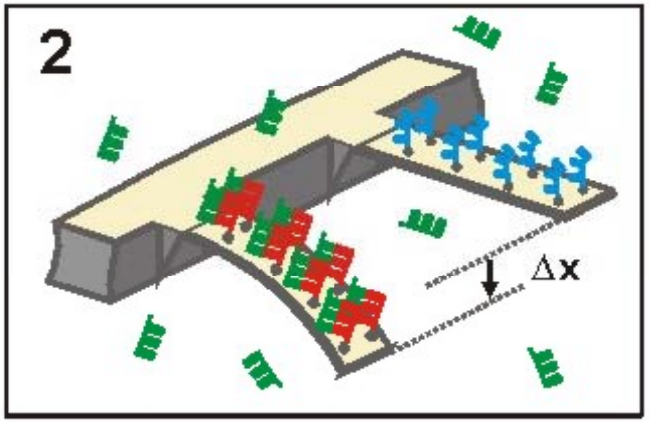

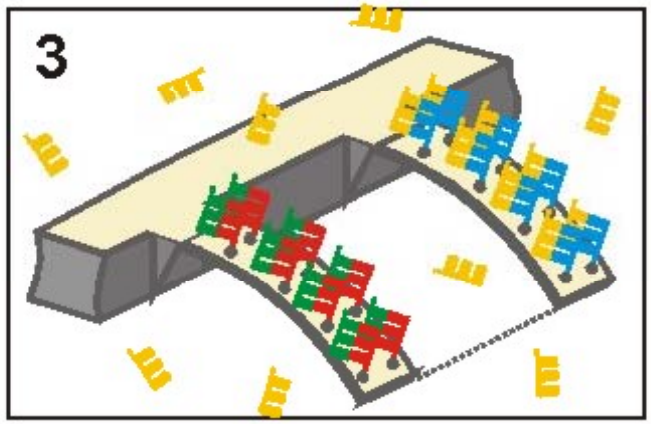

tial signal: lever 1 - lever 2

only one reactive surface

- bending of lever 1 increases differential signal
- bending of lever 2 decreases " "

Potential fields of Application

gas sensing

automotive applications

quality control (food, chemicals, air)

fragrance design

medical application

biochemical analysis

oenology

forensic investigations

drugs and explosives detection

astrobiology . . .

plications and examples

EMBRANE BASED SENSORS

MORESISTIVE GAS SENSORS - *Sensor design and cation*

ron ($9 \cdot 10^{15}$ cm^{-2}, 100 lanted and diffused boron doping from - diffusion (1050°C, 4 e p-n junction, 12 μm otropical stop etch

layer deposition and f the masking layer for etching of silicon

d configuration of a oped polysilicon layer.

sion could be to use the e high doped with boron t polysilicon resistor-

is deposed such as and the contacts at

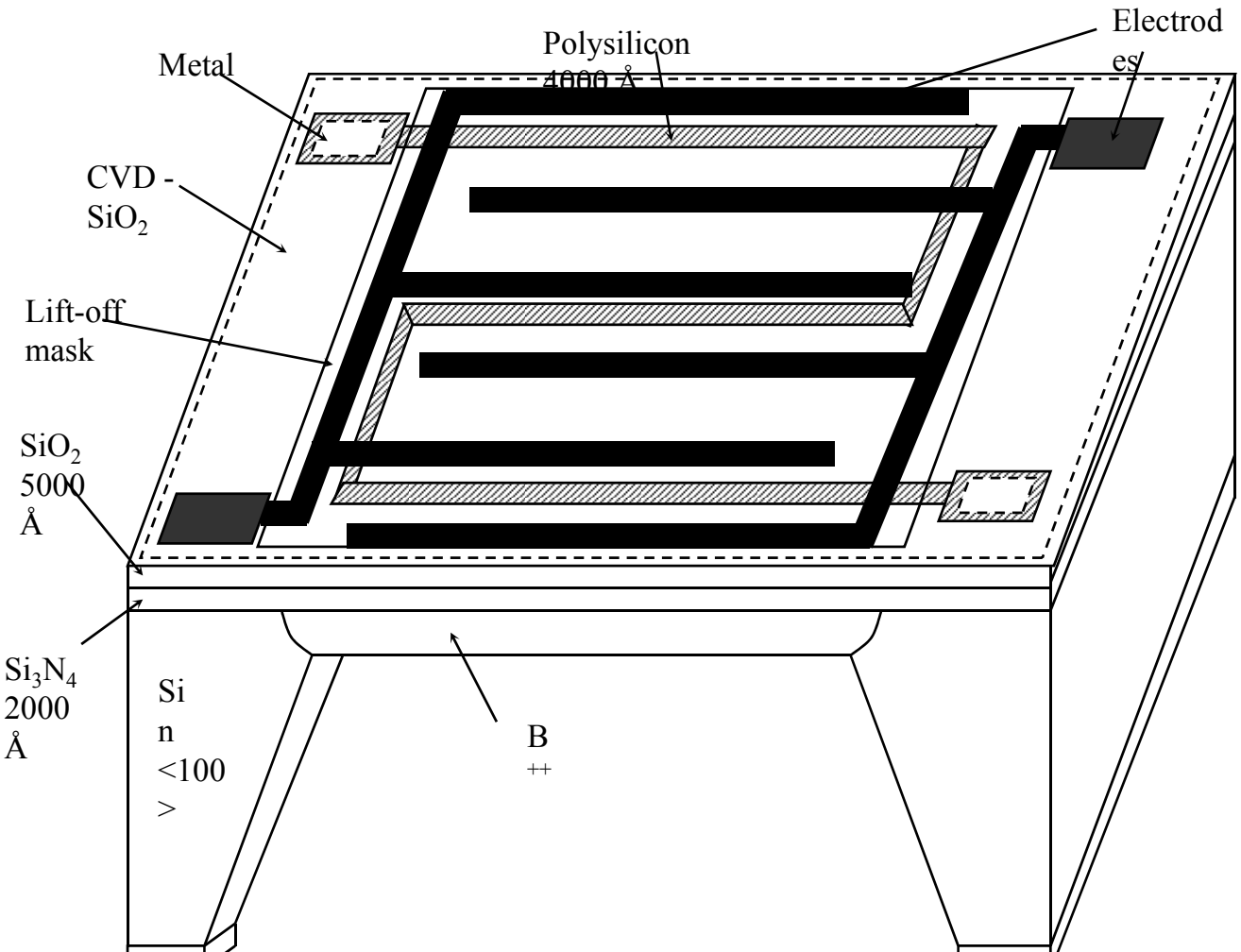

IORESISTIVE GAS SENSORS Phtalocyanine based – *riments -1*

nterdigitated electrodes, the resistor oring the chip temperature and the y bond pads are defined by ography above the insulated heater

(Cr-Au) was used as electrode to achieve a good contact with the The utilisation of Al as electrode give us, also, very good results.

sition and the configuration by side alignment of 2 μm sphosilicate glass (BPSG), as mask for the anisotropic etching, which

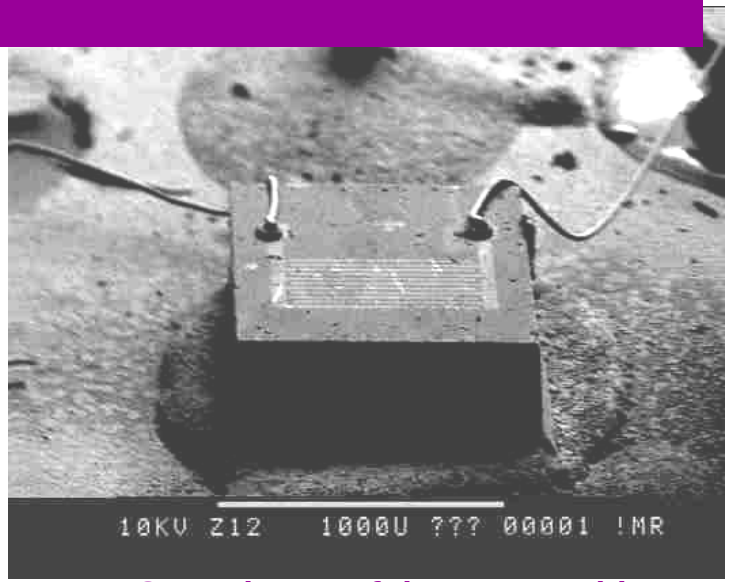

SEM picture of the sensor chip

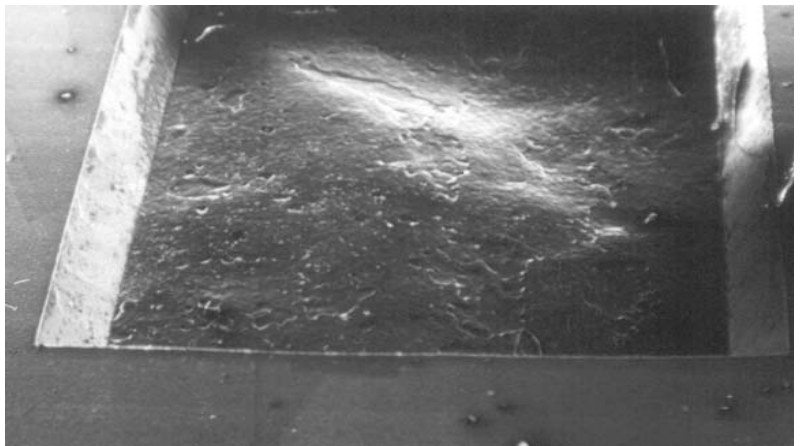

EMFET sensors

selective

Gas selective

Enzyme selective

Immuno-selective

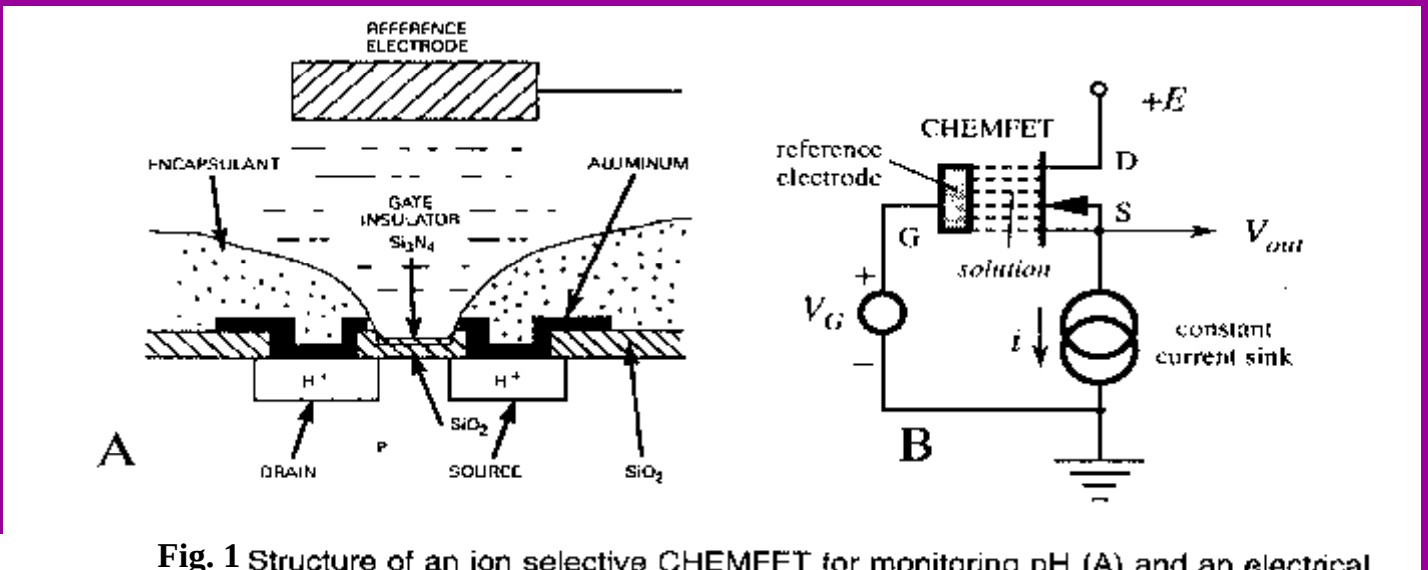

Fig. 1 Structure of an ion selective CHEMFET for monitoring pH (A) and an electrical

FET BASED SENSORS FOR MONITORING OF GASES

ct gas sensors are based on metal-insulator-semiconductor structures in metal gate is a catalyst for gas sensing. Typical catalytic metals used in this n are palladium, platinum, and iridium.

Sensors use the field effect transistors to detect chemical quantities. are biological and medical applications. The surface field effect is a desirable m for a generating potential that provides high chemical selectivity and . The CHEMFET is essentially an extended gate field effect transistor with the the transistor and the reference electrode

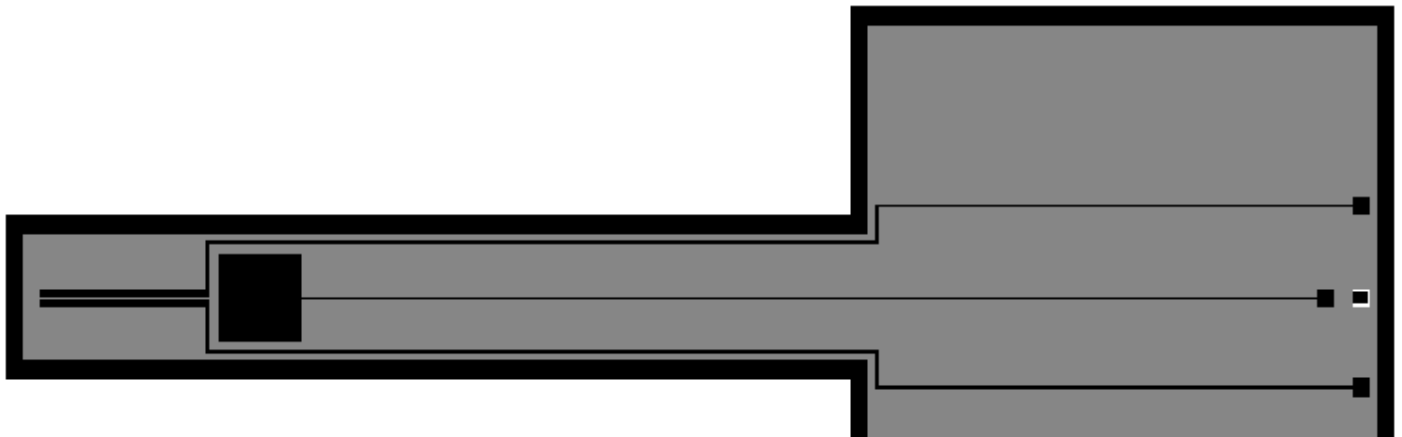

MANUFACTURING STEPS

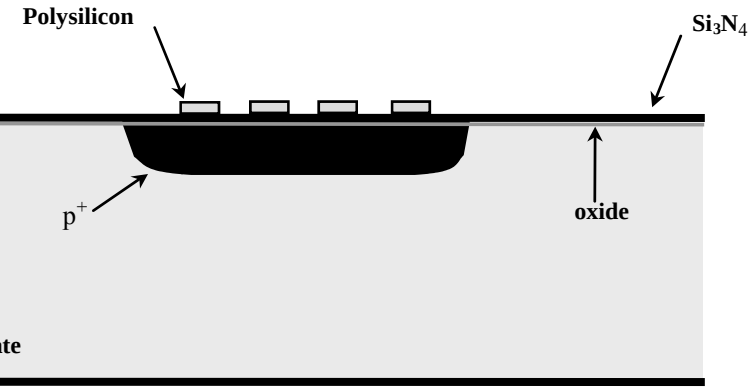

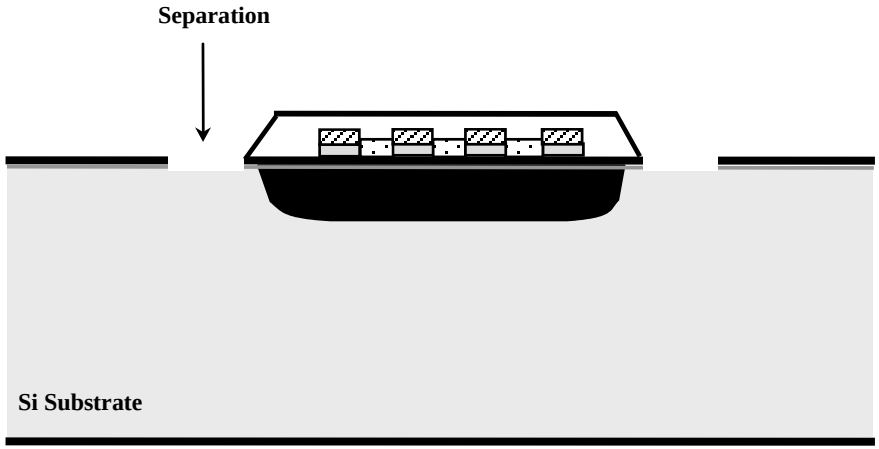

b

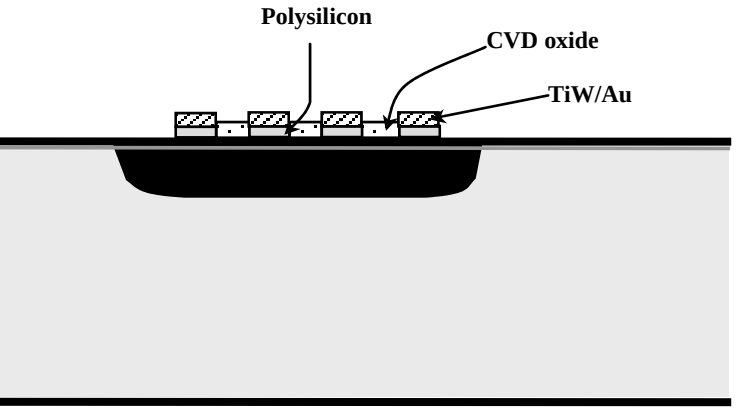

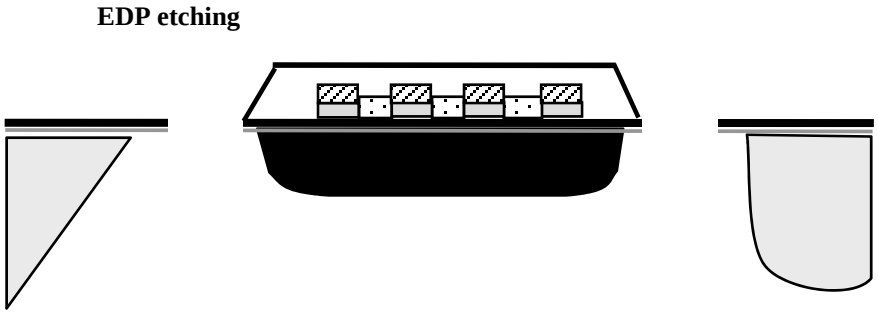

MICROMACHINED MICROPROBE -1

l micrograph of the body of the microprobe which hosts the electronics and allows the
ing at the external package is presented in fig.4. and the microprobe tip is presented in

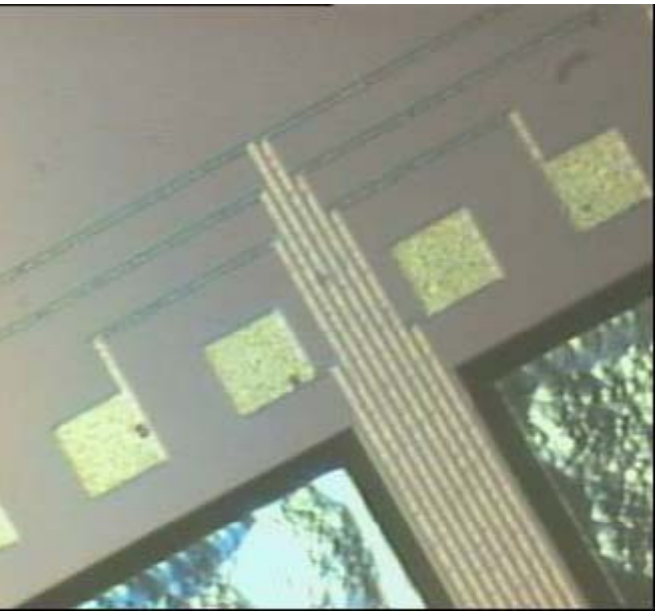

The body of the microprobe and the
ads (optical microphotography) after 5h
etching in EDP, 96 ^{0}C

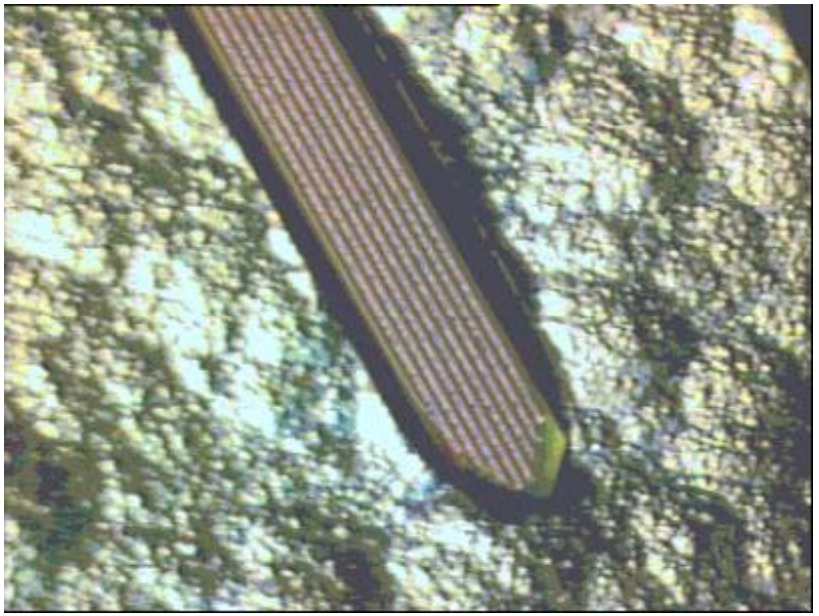

Fig.7.5. Optical microphotography (x100) of the
microprobe tip, after 5h etching in EDP, 96 ^{0}C

BASED BIOSENSORS FOR MONITORING OF THE Ca^{+2}, Mg^{+2}, IONS AND pH, IN VITRO AND IN VIVO -2

e microprobe ISFET biosensors

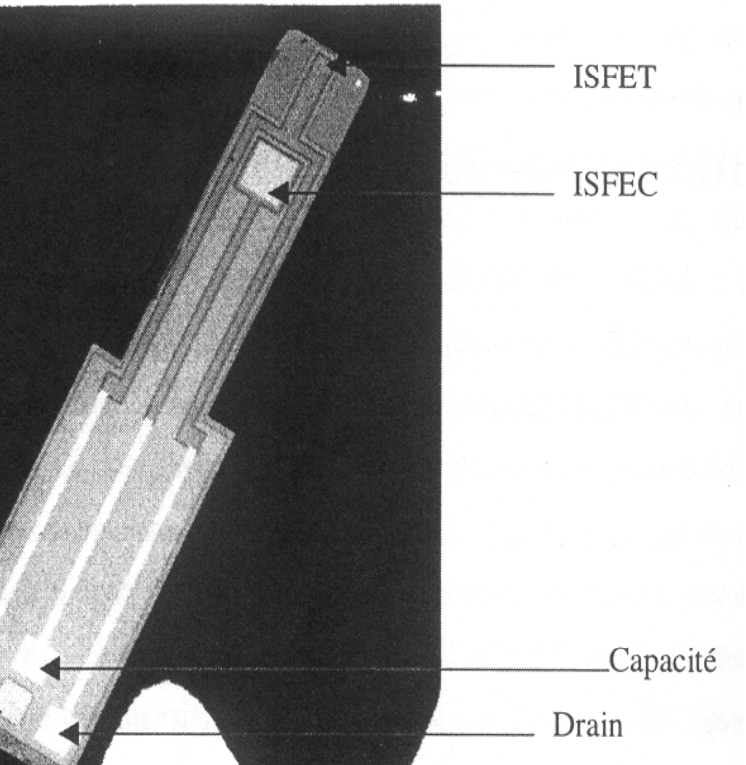

ISFET biosensor with integrated reference electrode

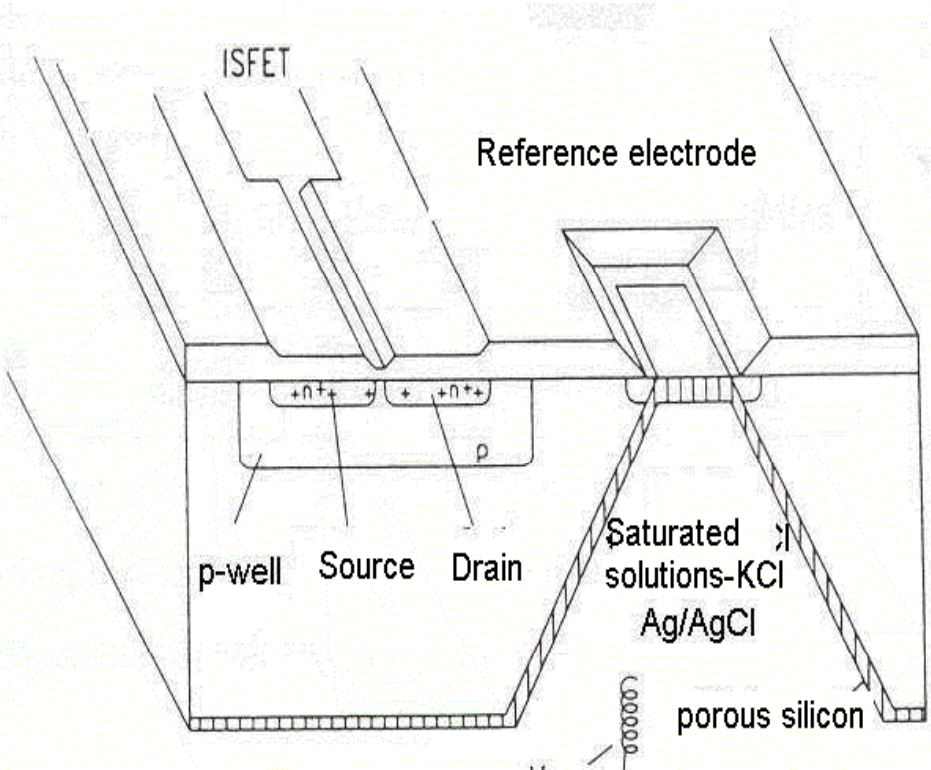

LYMER MICROMACHINING

Microfluidic channels

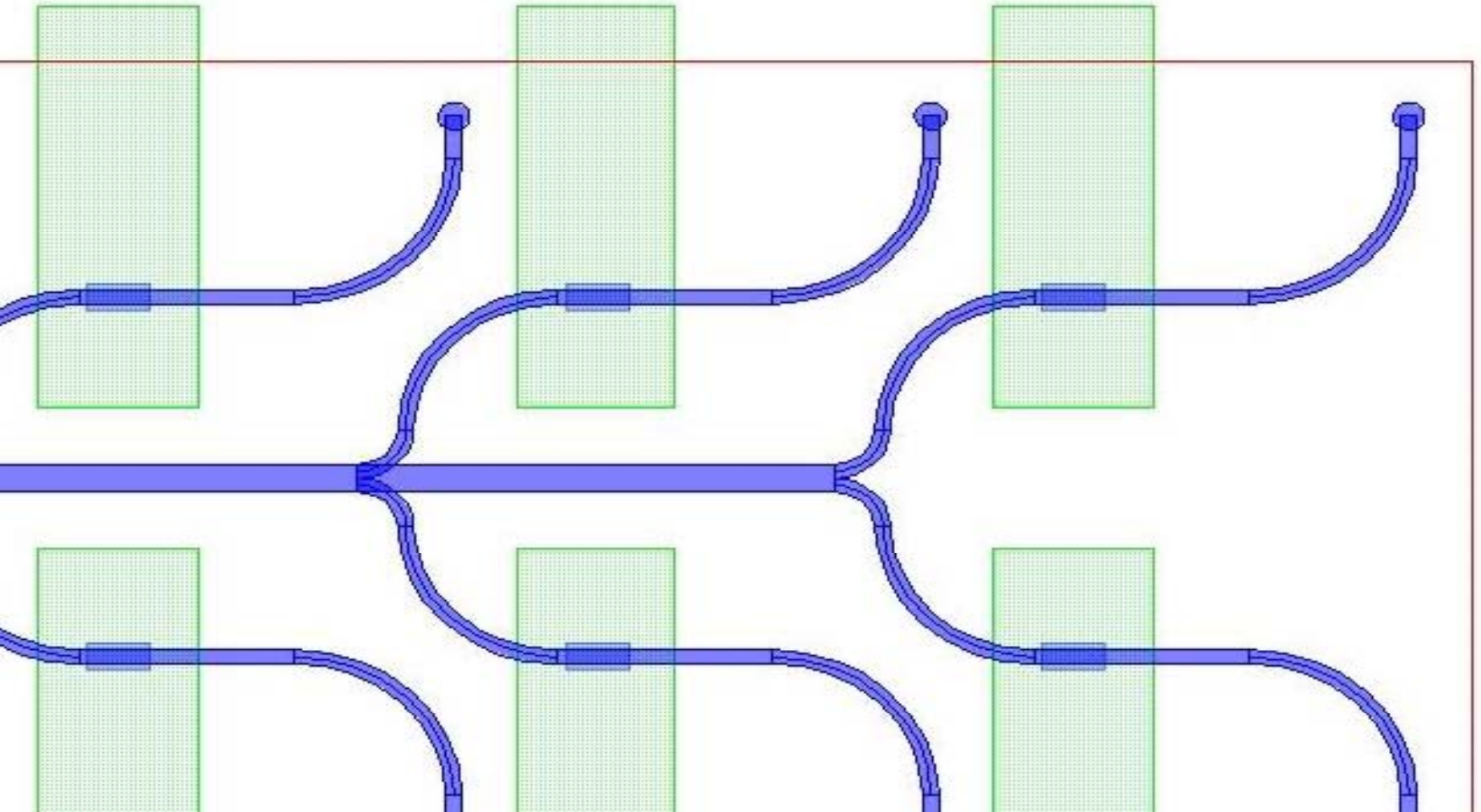

er Micromachined platform

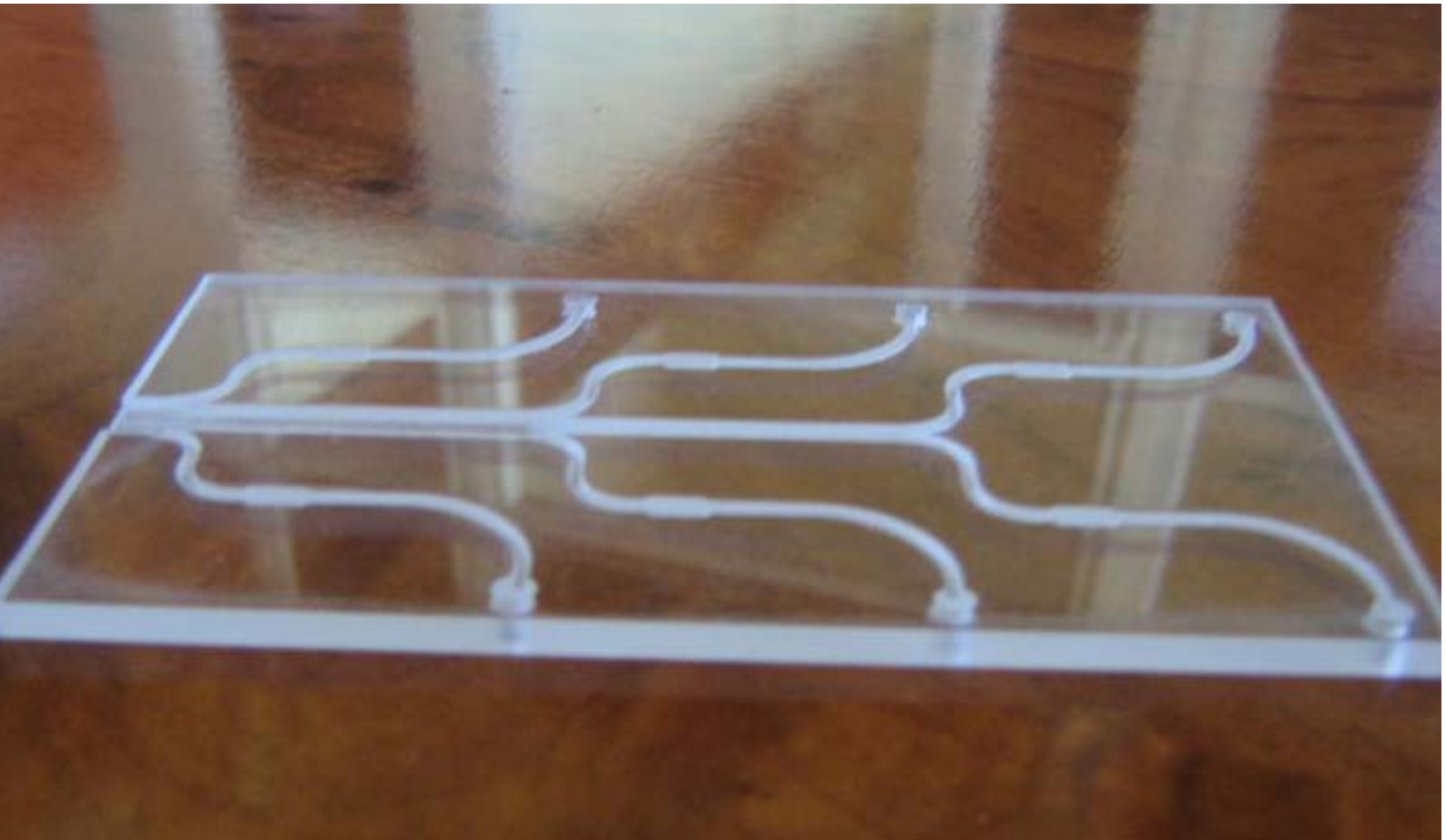

ss micromachining

- t etching (isotropic or anisotropic) of glass
- tal deposition+ lithography for sensor patterning
- sma treatment for resist removal
- sma treatment for surface functionalization

nsors platform

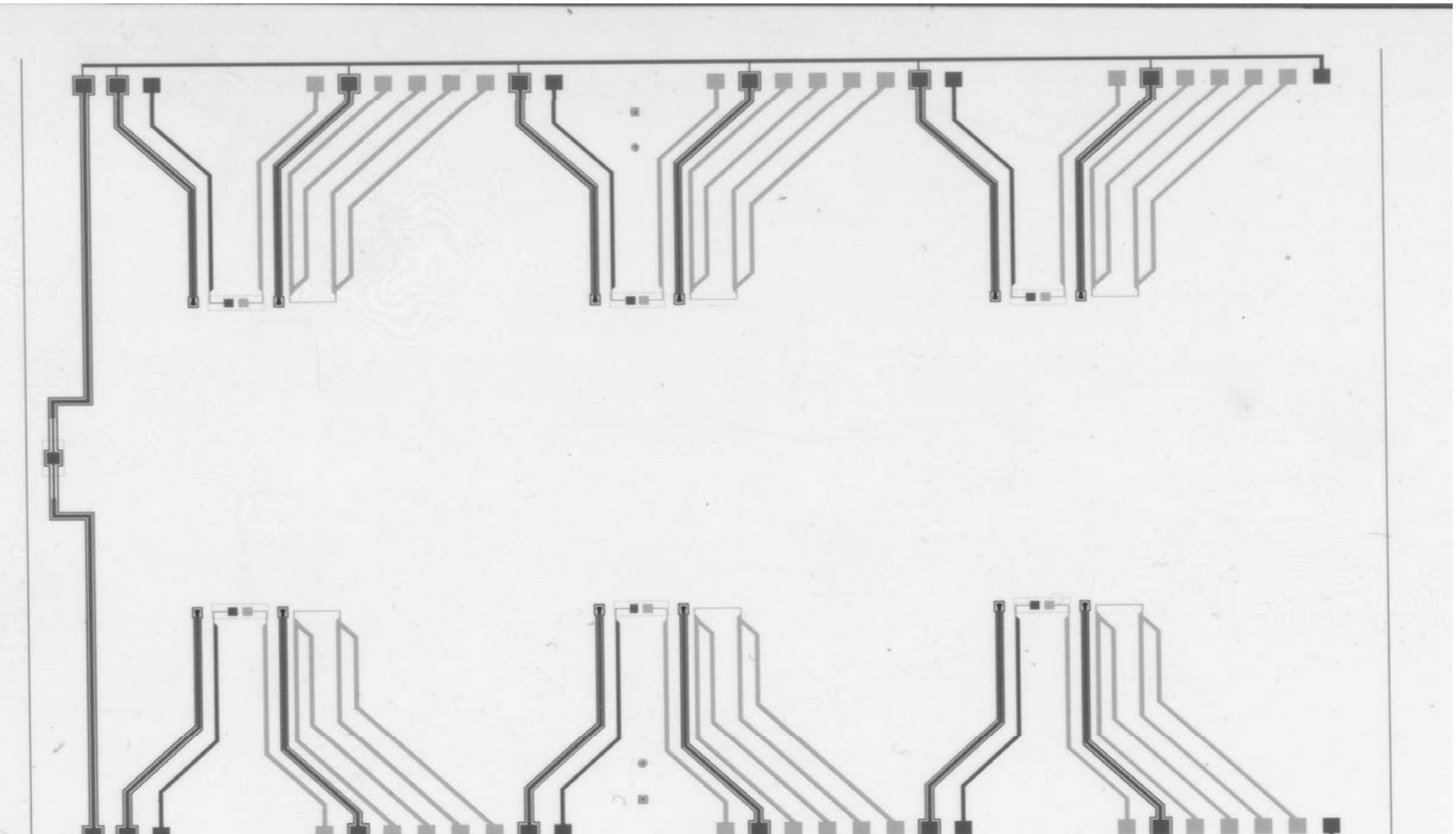

machining of ceramics

veloping a novel class of chemoresistive gas rs

aturized
cost
power consumption

g mixed techniques such as:

milling techniques;
uctive ceramic technology;
& thick film technology;
micromachining techniques

Design and technological steps

The sensor consists of an integrated heater and a platinum temperature sensor on top of a suspended membrane.

STEP A.
***Silicon bulk micromachining of electroceramic heater channels* (100 μm width) & subsequent filling with conducting ceramic**

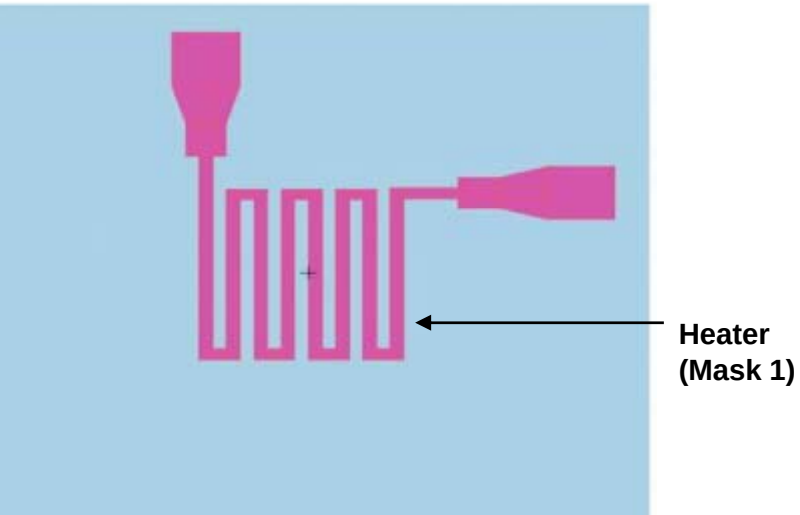

STEP B.
Deposition and configuration of an electric isolating layer **(SiO_2 or ceramic).**

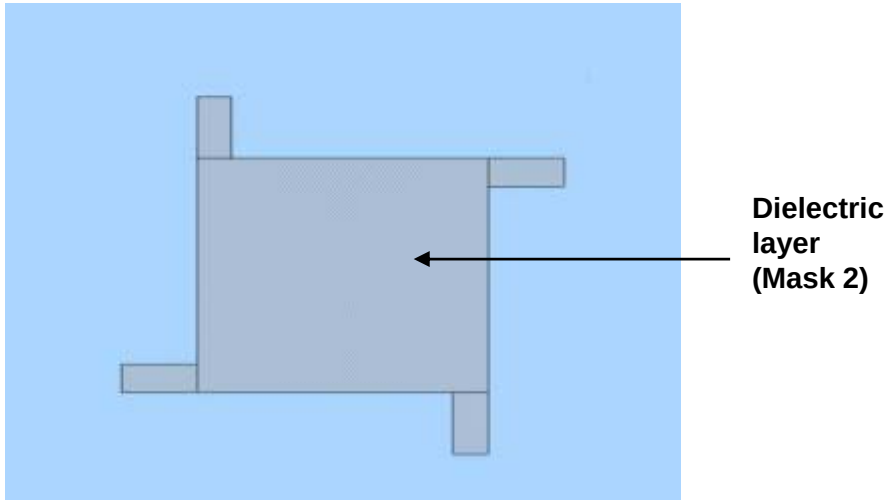

Design and technological steps

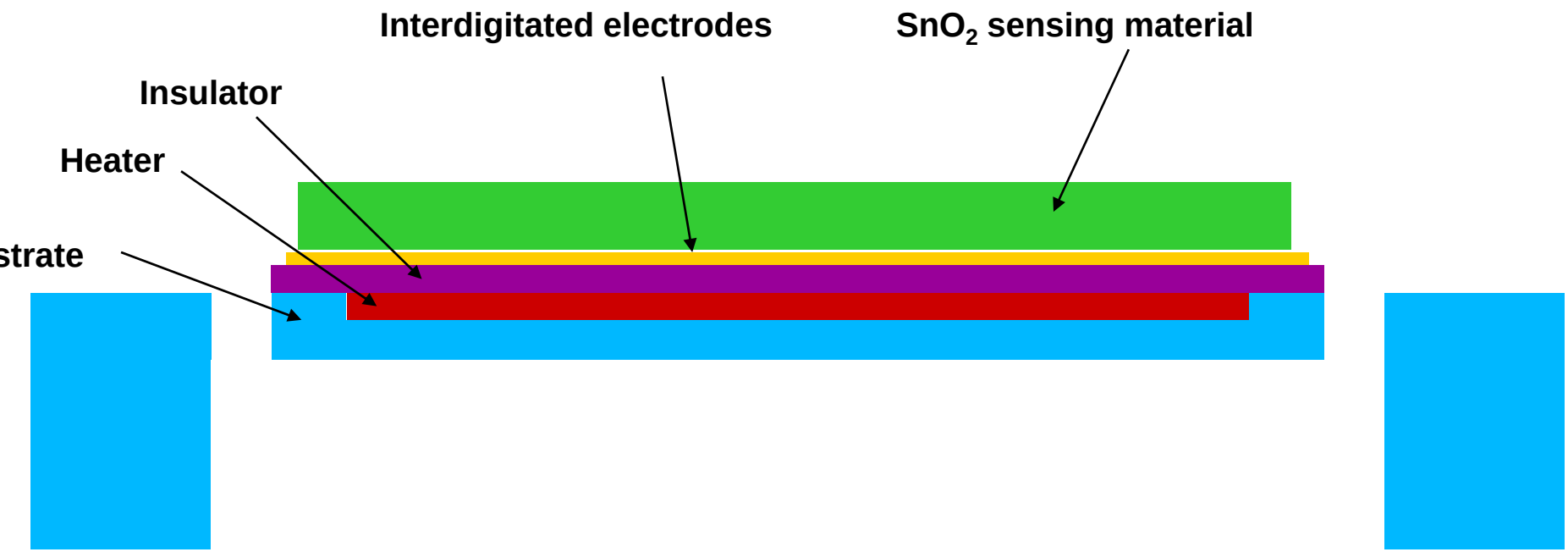

Fig.8. Mask 6 - Membrane releasing

Manufacturing Steps

ining the heater groove

g the groove with AuPtPd paste

ning and release of the heater. The releasing ation was performed first by machining the pridges around the heater. This operation completed by traversing the 0.5x2 mm ngles several times until the full thickness e wafer was machined, resulting in a ngular hole.

hinning of the ceramic substrate back side. was performed by “scanning” the 3x3 mm with the laser beam as shown in the Figure, e the lateral step size (s) was 6 μm.

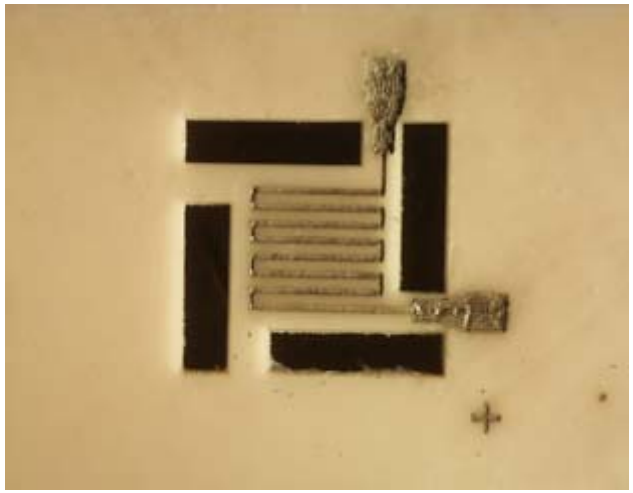

The suspended heating element

ent of the thermal properties

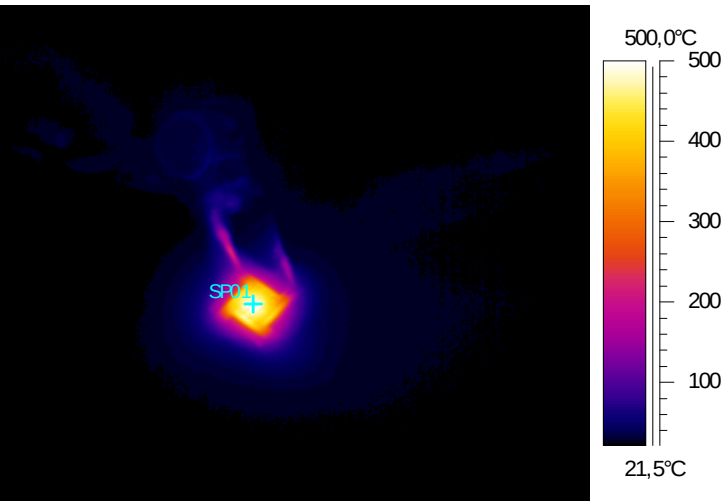

e heat distribution from the released ating element using FLIR 40

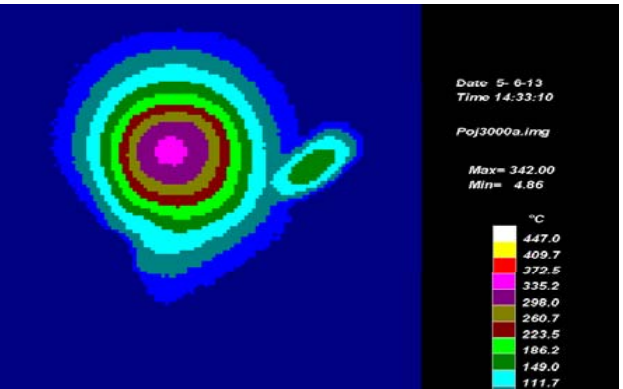

The temperature is uniform at the released area and the outside area at least 400 °C lower temperature.

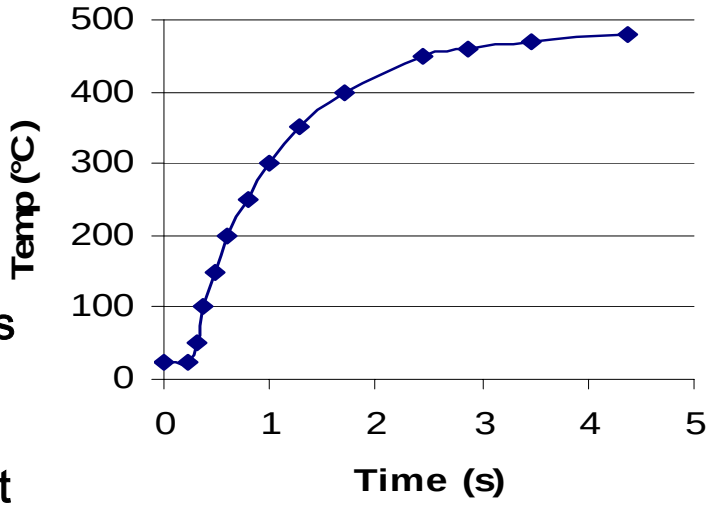

The power-on curve for the released heater element.

The input power was 1,1 W and this should be compared with the non-released heater element

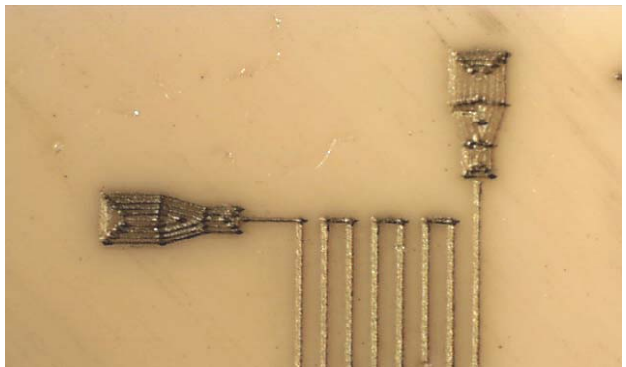

es

istic, Sensor Technology and Devices, Artech House, Boston, 1994, pp 67-68

. Seidel, L. Csepregi, A. Heuberger, H. Baumgärtel, Anisotropic Etching of Crystalline n Alkaline Solutions, Journal of the Electrochemical Society, 137 (1990), 3612-3632

Moldovan, R. Iosub, D. Dascalu, Gh. Nechifor, C. Radu, An investigation of an Alkaline for Silicon Anisotropic Etching, Abstract, Workshop of Physical Chemistry of Wet Etching of Silicon, Holten, 1998, pp 21-22

D. Gutsche, B. Dhawan, K. Hyum No, R. Mathukrishnan, Calixarenes. 4. The Synthesis, ization, and Properties of the Calixarenes from p-tert- Butylphenol, J. Am. Chem Soc.,), 3782-3792

Shinkai, K. Araki, J. Shibata, D. Tsungawa, O. Manabe, Autoaccelerative Diazo Coupling x[4] arene: Substituent Effects on the Unusual Co-operativity of the OH Groups, J. Chem. in Trans.1 (1990), 3333-3337

inus Pauling, General Chemistry, W.H. Freeman and Company, San Francisco, 1970, in Bucharest 1972, pp. 461-462

Sato, M. Shikida, Y. Matsushima, T. Yamashiro, K. Asaumi, Y. Iriye, M. Tamamoto,

, M. L. Reed, H. Han and R. Boudreau, Mechanism of Etch Hillock Formation, Journal ectromechanical Systems, 5 (1996), 65-71

. M. M. C. Bressers, J. J. Kelly, J. G. E. Gardeniers and M. Elwenspoek, Surface gy of p-Type (100) Silicon Etched in Aqueous Alkaline Solution, Journal of the mical Society, 143 (1996), 1744-1750

Elwenspoek, Stationary Hillocks on Etching Silicon, Proceedings, The Ninth hanics Europe Workshop MME'98, Ulvik in Hardanger, Norway,June 3-5, 1991, pp 70-

Schröder, E. Obermeier, A. Steckenborn, Formation, prevention and removal of mids on KOH etched {100} silicon, Proceedings, The Ninth Micromechanics Europe MME'98, Ulvik in Hardanger, Norway, June 3-5, 1991, pp 28-31

be, A Contamination-Free Microstructure in a Humid Environment by Means of a on of Hydrophilic and Hydrophobic Surfaces, Journal of Microelectromechanical (1998), 94-101